ANTIOXIDANTS & REDOX SIGNALING
Volume 23, Number 5, 2015

DOI: 10.1089/ars.2014.6202

FORUM ORIGINAL RESEARCH COMMUNICATION

Discovery of GSK2795039, a Novel Small Molecule NADPH Oxidase 2 Inhibitor

Kazufumi Hirano,[1,*] Woei Shin Chen,[1,*] Adeline L.W. Chueng,[1] Angela A. Dunne,[1] Tamara Seredenina,[2] Aleksandra Filippova,[2] Sumitra Ramachandran,[1] Angela Bridges,[3] Laiq Chaudry,[3] Gary Pettman,[3] Craig Allan,[3] Sarah Duncan,[1] Kiew Ching Lee,[1] Jean Lim,[1] May Thu Ma,[1] Agnes B. Ong,[1] Nicole Y. Ye,[1] Shabina Nasir,[1] Sri Mulyanidewi,[1] Chiu Cheong Aw,[1] Pamela P. Oon,[1] Shihua Liao,[4] Dizheng Li,[4] Douglas G. Johns,[5] Neil D. Miller,[1] Ceri H. Davies,[1] Edward R. Browne,[1] Yasuji Matsuoka,[1] Deborah W. Chen,[1] Vincent Jaquet,[2,*] and A. Richard Rutter[1,*]

Abstract

Aims: The NADPH oxidase (NOX) family of enzymes catalyzes the formation of reactive oxygen species (ROS). NOX enzymes not only have a key role in a variety of physiological processes but also contribute to oxidative stress in certain disease states. To date, while numerous small molecule inhibitors have been reported (in particular for NOX2), none have demonstrated inhibitory activity *in vivo*. As such, there is a need for the identification of improved NOX inhibitors to enable further evaluation of the biological functions of NOX enzymes *in vivo* as well as the therapeutic potential of NOX inhibition. In this study, both the *in vitro* and *in vivo* pharmacological profiles of GSK2795039, a novel NOX2 inhibitor, were characterized in comparison with other published NOX inhibitors. ***Results:*** GSK2795039 inhibited both the formation of ROS and the utilization of the enzyme substrates, NADPH and oxygen, in a variety of semirecombinant cell-free and cell-based NOX2 assays. It inhibited NOX2 in an NADPH competitive manner and was selective over other NOX isoforms, xanthine oxidase, and endothelial nitric oxide synthase enzymes. Following systemic administration in mice, GSK2795039 abolished the production of ROS by activated NOX2 enzyme in a paw inflammation model. Furthermore, GSK2795039 showed activity in a murine model of acute pancreatitis, reducing the levels of serum amylase triggered by systemic injection of cerulein. ***Innovation and Conclusions:*** GSK2795039 is a novel NOX2 inhibitor that is the first small molecule to demonstrate inhibition of the NOX2 enzyme *in vivo*. *Antioxid. Redox Signal.* 23, 358–374.

Introduction

NADPH oxidase (NOX) enzymes are major sources of reactive oxygen species (ROS) and mediate signaling events in a variety of physiological processes, such as hormone biosynthesis, cell signaling, and microbial killing (7). The NOX enzyme family comprises multiple isoforms, including NOX1–5 and dual oxidases (DUOX1 and DUOX2) (38). While the isoforms differ in their tissue distribution, subunit composition, domain structure, and mechanism of activation, all seven isoforms contain homologous catalytic domains and share a common biochemical function, that is, catalysis of ROS generation (7, 37). The best-characterized member of the NOX enzyme family is the NOX2 isoform, which was originally identified as the enzyme responsible for the respiratory burst in phagocytic cells, a critical cellular

[1]Neural Pathways Discovery Performance Unit, Neurosciences Therapeutic Area, GlaxoSmithKline, Biopolis, Singapore.
[2]Department of Pathology and Immunology, Medical School, Centre Médical Universitaire, University of Geneva, Geneva, Switzerland.
[3]Platform Technology & Sciences Department, GlaxoSmithKline, Stevenage, United Kingdom.
[4]Neuroimmunology Discovery Performance Unit, Neurosciences Therapeutic Area, GlaxoSmithKline, Shanghai, China.
[5]Metabolic Pathways and Cardiovascular Therapeutic Area, GlaxoSmithKline, King of Prussia, Pennsylvania.
*These authors contributed equally to the authorship of this publication.

Innovation

GSK2795039 directly inhibits NADPH oxidase 2 (NOX2) as demonstrated by its inhibition of reactive oxygen species (ROS) production and NADPH consumption in a recombinant NOX2 system. It is selective for NOX2 as shown in NOX-specific cell-based assays addressing oxygen consumption and horseradish peroxidase-independent ROS detection *in vitro*. GSK2795039 shows *in vivo* target engagement in the periphery as well as protective effects in a model of acute pancreatitis. The present study rigorously demonstrates that GSK2795039 is a novel small molecule NOX2 inhibitor that can be used to explore both NOX2 biology *in vivo* and the therapeutic potential of NOX2 inhibition in disease.

event underlying innate immune defense. The central molecular component of the NOX2 enzyme is a membrane-localized, glycosylated catalytic subunit, $gp91^{phox}$, which coassembles with a second membrane-associated subunit, $p22^{phox}$. There are four cytosolic regulatory subunits, $p47^{phox}$, $p67^{phox}$, $p40^{phox}$, and Rac, which, upon activation, translocate to the membrane and associate with the $gp91^{phox}$/$p22^{phox}$ complex (50). Once formed, the NOX2 enzyme catalyzes the conversion of cytoplasmic NADPH to $NADP^+$ with concomitant transfer of electrons through the flavin adenine dinucleotide (FAD) domain and iron-heme prosthetic groups to oxygen molecules, resulting in formation of superoxide anions in the extracellular or intraphagosomal space (7, 37).

In addition to their role in normal physiology, several lines of evidence suggest that chronic activation or overproduction of cytotoxic ROS by NOX enzymes leads to oxidative stress, a key pathological mechanism thought to underlie various disease states (29, 36, 46), such as atherosclerosis (5, 32, 56), diabetic nephropathy (25, 28), acute lung injury (29), pulmonary fibrosis (3, 10), and amyotrophic lateral sclerosis (66). Numerous animal studies using genetic ablation of $gp91^{phox}$ and/or $p47^{phox}$ support the hypothesis that pharmacological inhibition of NOX2 may be a therapeutic strategy (15). However, complete abrogation of NOX2 is known to lead to increased infections and increased sensitivity to autoimmune disorders and should be carefully considered for such treatments.

Throughout the last decade, efforts to validate the relative contribution of specific NOX enzymes to either normal physiological processes or to pathological states have been made primarily *via* the characterization of genetic knockout animals or with the use of peptide-based inhibitors (12, 37). However, both approaches have different caveats such as the potential for compensatory mechanisms in constitutive knockout mice and the limited biodistribution and efficacy of peptides. As such, the development of small-molecule NOX inhibitors is not only needed to characterize NOX biology but also to validate their potential as therapeutic agents (3).

To date, a number of small molecules have been shown to block ROS production in primary neutrophils or related cell lines and hence reported as NOX inhibitors (3, 31). However, for most of these inhibitors, a full understanding of their mode of action, selectivity, *in vivo* pharmacokinetics, and pharmacodynamics is lacking; therefore, their utility in characterizing NOX2 biology in complex biological systems is limited. Hence, we undertook a screening campaign to identify novel small molecule NOX2 inhibitors with the aim of identifying a potent inhibitor that could specifically inhibit the NOX2 enzyme following systemic administration in rodents.

To truly validate a small molecule as an NOX inhibitor, extensive characterization of its pharmacology is required to prove that apparent activity in enzyme and cell-based assays is specific to the particular NOX enzyme and is not due to free radical scavenging, interference with the ROS detection reagents, or inhibition of upstream pathways. The commonly used inhibitor, diphenyleneiodonium (DPI), blocks ROS production in phagocytes *via* accepting an electron from flavin. This enables DPI to interfere not only with NOX but also with other flavin-dependent enzymes, such as nitric oxidase synthase, xanthine oxidase, mitochondrial complex I, and cytochrome P-450 reductase (49). In addition to its broad selectivity, the utility of DPI as an *in vivo* tool to evaluate NOX biology is limited by its irreversible binding to flavin, low solubility, and high toxicity in rodents ($LD_{50} <$ 10 mg/kg) (20, 49).

Another small molecule, apocynin, has also been commonly used as a tool inhibitor to evaluate the function of NOX2 in biological systems. As a natural methoxy-substituted catechol isolated from *Picrorhiza kurroa* (59), apocynin showed efficacy in a wide range of rodent disease models, including hypertension (47, 52), diabetic nephropathy (24), cardiac hypertrophy (4, 41), retinal vascular inflammation (1), and stroke (22, 62). While apocynin has been shown to inhibit the phagocyte respiratory burst in some cellular assays (57), its mechanism of action is still a matter of debate because it also has radical scavenging properties and does not inhibit NOX2 in a cell-free enzyme system (27, 31).

The pharmacology of other small molecule NOX2 inhibitors *in vivo* has not been well defined. As such, there is a clear need for the development of directly acting NOX enzyme inhibitors that are suitable for testing *in vivo* to accurately define the biological functions of NOX enzymes and to assess their potential as therapeutic drug targets.

In this study, we report the pharmacological characterization of GSK2795039, a novel small molecule that is a potent NOX2 enzyme inhibitor in various *in vitro* and *in vivo* systems. In parallel, we have characterized other reported NOX inhibitors and highlighted apparent differences in their pharmacology. Our study highlights the potential flaws inherent to the use of ROS detection systems and emphasizes the need for several unrelated assays to measure NOX activity. Finally, we demonstrate that GSK2795039 inhibits the NOX2 enzyme following systemic dosing in rodents and is therefore a suitable tool molecule to further evaluate the pathophysiological role of NOX2.

Results

GSK2795039 is a potent inhibitor of NOX2 in cell-free and whole-cell assays

GSK2795039 (Fig. 1), *N*-(1-Isopropyl-3-(1-methylindolin-6-yl)-1*H*-pyrrolo[2,3-*b*]pyridin-4-yl)-1-methyl-1*H*-pyrazole-3-sulfonamide, was discovered following a high-throughput screen and subsequent lead optimization campaign to identify inhibitors of the NOX2 enzyme. GSK2795039 is a novel 7-azaindole structure wherein sulfonamide functionality is

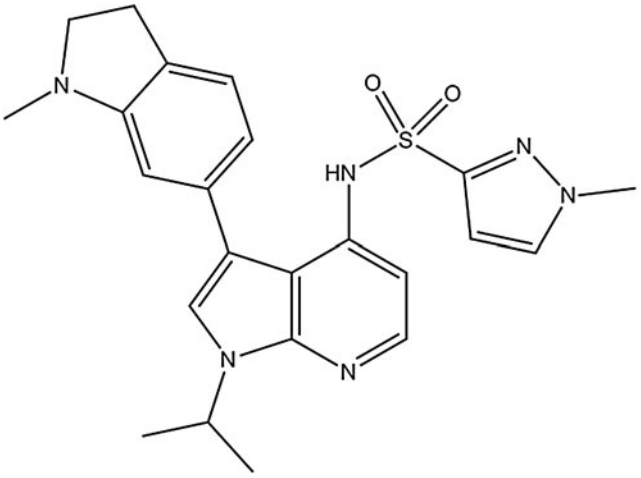

FIG. 1. Structure of GSK2795039.

critical for its NOX2 activity. This feature is unique to GSK2795039 and was an early indication of its differentiated mode of action from other reported NOX inhibitors.

A number of assays were developed to assess the pharmacological activity of test compounds on the NOX2 enzyme and to counter screen for nonspecific and off-target effects that may manifest as apparent inhibitory activity in the enzyme assays. The primary assay utilized a semirecombinant NOX2 enzyme system using baby hamster kidney (BHK) cell membranes expressing $gp91^{phox}$ and purified recombinant cytosolic proteins. The enzyme was activated with arachidonic acid in combination with the horseradish peroxidase (HRP)/Amplex Red method of ROS detection. This assay format was chosen for a number of reasons: a high signal:noise ratio, the possibility to use a recombinant cell-free assay system rather than a whole-cell-based assay to increase the chances of identifying direct inhibitors of the NOX2 enzyme, and the possibility of miniaturization of the assay to a 1536-well plate format.

As shown in Figure 2A and B and summarized in Table 1, GSK2795039 and the positive control DPI fully inhibited NOX2-mediated activation of HRP/Amplex Red with pIC_{50} values of 6.57 ± 0.17 and 7.07 ± 0.25, respectively. To confirm that this activity was not due to inhibition of HRP activity or direct scavenging of ROS, we used additional semirecombinant cell-free NOX2 enzyme assays using the ROS detection reagents, Oxyburst Green and water-soluble tetrazolium salt1 (WST-1), whereas a complementary assay monitored the time-dependent depletion of the enzyme

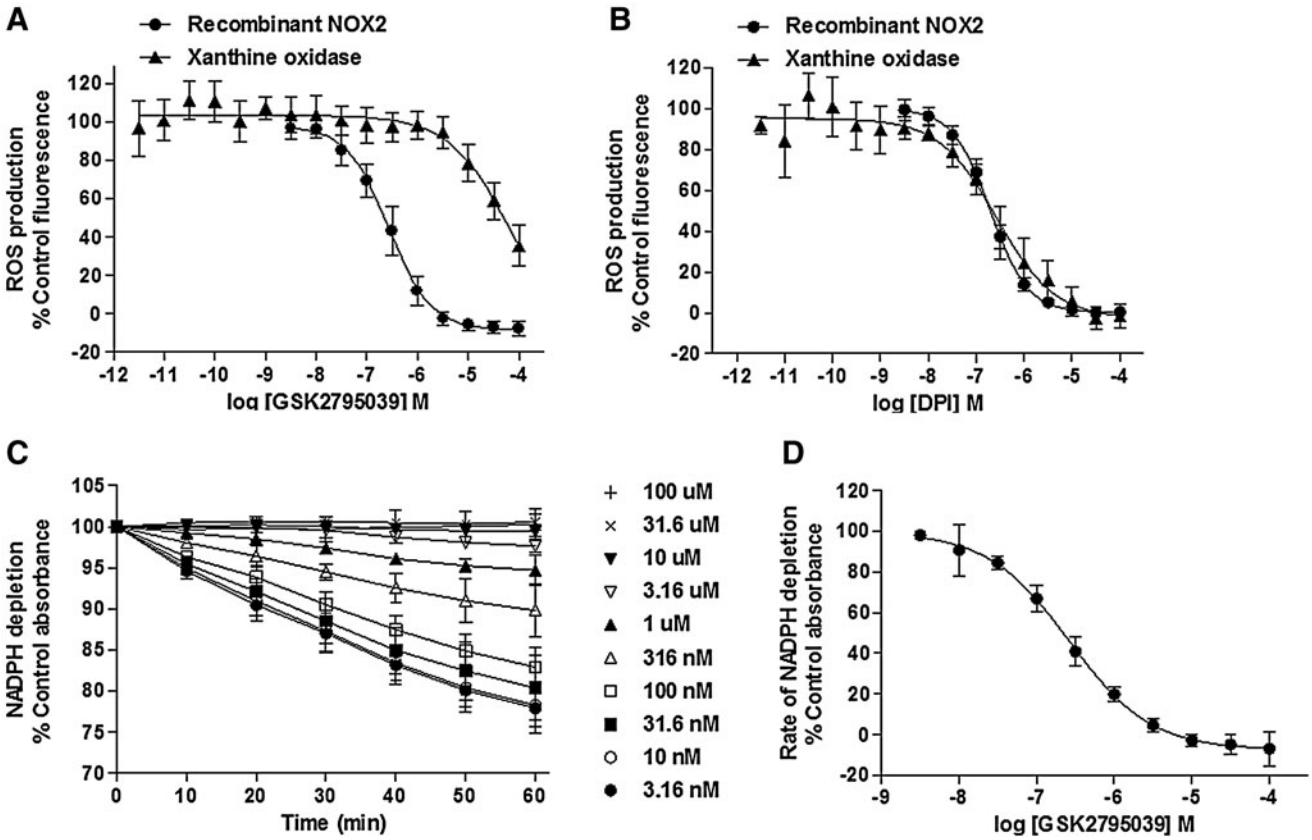

FIG. 2. Effect of GSK2795039 in cell-free assays. (A) Effect of GSK2795039 on ROS production in recombinant NOX2 and xanthine oxidase assays. **(B)** Effect of DPI on ROS production in semirecombinant NOX2 and xanthine oxidase assays. **(C)** Representative kinetic profile of GSK2795039 in the NADPH substrate depletion assay. 100% = no change in rate of reaction. **(D)** Concentration response curve of GSK2795039 in the NADPH substrate depletion in recombinant NOX2 assay. All NOX2 assays used BHK-gp91 cell membranes. All data points were normalized to maximum enzyme activity of the vehicle-treated control. Data are the mean ± standard deviation of all replicate experiments (*n* listed in Table 1), except where indicated as representative. BHK, baby hamster kidney; DPI, diphenyleneiodonium; NOX2, NADPH oxidase 2; ROS, reactive oxygen species.

Table 1. Summary Showing pIC_{50} Values for GSK2795039, DPI, Apocynin, VAS2870, Shionogi 2, Naloxone, ML171, Celastrol, and Suramin as Determined in the Different Cell-Free Enzyme Assays

		Recombinant NOX2 enzymes			*Other enzyme assays*	
Test compounds	*ROS production HRP/ Amplex Red*	*ROS production Oxyburst*	*ROS production WST-1*	*Substrate depletion NADPH*	*Xanthine oxidase HRP/Amplex Red*	*PKCB II*
GSK2795039	6.57 ± 0.17 (10)	6.27 ± 0.13 (5)	6.18 ± 0.11 (3)	6.60 ± 0.13 (>10)	4.54 ± 0.16 (10)	< 4.6 (4)
DPI	7.07 ± 0.25 (>10)	7.64 ± 0.29 (5)	ND	7.55 ± 0.24 (>10)	6.57 ± 0.21 (>10)	ND
Apocynin	4.09 ± 0.12 (8)[a]	< 4 (5)	ND	< 4 (4)	4.04 ± 0.07 (3)	ND
VAS2870	< 4 (10)	< 4 (5)	ND	< 4 (4)	< 4 (3)	< 4.6 (2)
Shionogi 2	< 4 (4)	4.73 ± 0.08 (5)	ND	< 4 (4)	< 4 (3)	7.6 ± 0.27 (>10)
Naloxone	< 4 (4)	< 4 (4)	ND	< 4 (4)	< 4 (3)	> 5 (4)
ML171	6.47 ± 0.12 (4)	6.60 ± 0.21 (4)	ND	< 4 (4)	< 4 (3)	< 4.6 (2)
Celastrol	5.24 ± 0.26 (4)	< 4 (5)[b]	ND	5.45 ± 0.16 (4)	< 4 (3)	< 4.6 (2)
Suramin	5.69 ± 0.07 (4)	5.73 ± 0.11 (5)	ND	5.89 ± 0.04 (4)	< 4 (3)	< 4.3 (8)

Data are expressed as mean ± standard deviation (*n*). Symbol (<) indicates that compound was inactive and/or showed less than 50% inhibition at top concentrations.

[a]Indicates that compound showed less than 50% inhibition at top concentrations in some replicate experiments, and a value of 4 was used to calculate the population mean.

[b]Indicates that interference of the test compound with the reagent was observed potentially obscuring a real pharmacological effect.

DPI, diphenyleneiodonium; HRP, horseradish peroxidase; ND, not done; NOX2, NADPH oxidase 2; PKCB II, protein kinase C beta2; ROS, reactive oxygen species; WST-1, water-soluble tetrazolium salt1.

substrate, NADPH. WST-1 is a formazan salt specifically reduced by the superoxide anion. Its use for detection of NOX activity was elegantly validated by Tan and Berridge (61) who highlighted its improved sensitivity over cytochrome C for measuring NOX activity. Specificity for NOX2-dependent superoxide detection by Oxyburst Green and WST-1 assays is documented in Supplementary Figure S1 (Supplementary Data are available online at www.liebertpub.com/ars). GSK2795039 fully inhibited NOX2 in both assays (pIC_{50} values shown in Table 1).

The measurement of substrate depletion in the NADPH absorbance assay is a key assay technique to characterize NOX inhibitors because it is not prone to the potential artifacts commonly associated with ROS detection methodologies. As shown in Figure 2C, the concentration of NADPH measured *via* absorbance at 340 nm declined in a linear manner over 60 min in the presence of activated NOX2 enzyme. Both GSK2795039 and DPI concentration dependently decreased the rate of NADPH utilization with pIC_{50} values of 6.60 ± 0.13 and 7.55 ± 0.24, respectively (Fig. 2C, D and Table 1).

GSK2795039 and DPI were also tested for inhibitory activity against another oxidase enzyme, purified xanthine oxidase, using the HRP/Amplex Red method of ROS detection. In contrast to DPI, which inhibited xanthine oxidase with a pIC_{50} of 6.57 ± 0.21, GSK2795039 was only a weak inhibitor with a pIC_{50} of 4.54 ± 0.16 exhibiting >100-fold selectivity for NOX2 over xanthine oxidase (Fig. 2A, B, and Table 1). In addition, GSK2795039 only weakly inhibited endothelial nitric oxide synthase (eNOS) (<50% when tested at 100 μM, Table 2).

To evaluate the cellular activity of GSK2795039, differentiated HL60 cells and human peripheral blood mononucleated cells (PBMCs) were stimulated with phorbol 12-myristate 13-acetate (PMA) in the presence and absence of compound, using L-012 or Oxyburst Green to detect ROS production. PMA (12 n*M*) stimulation of HL60 cells caused a time-dependent increase in L-012 luminescence over 60 min that was fully inhibited by GSK2795039 and DPI with pIC_{50} values of 6.74 ± 0.17 and 6.84 ± 0.22, respectively (Fig. 3A, B, and Table 3). Similar pIC_{50} values (6.73 ± 0.16 and 6.49 ± 0.18, respectively) were obtained when Oxyburst Green was used as the ROS detection reagent. In PBMCs, GSK2795039 inhibited ROS production as measured with L-012 (Fig. 3C) with a pIC_{50} value of 6.60 ± 0.08 ($n = 4$); an effect consistent with potent inhibition of the NOX2 enzyme. We also evaluated potential cytotoxic effects of GSK2795039 in cultured cells (human embryonic kidney [HEK] 293 cells), but did not observe any significant toxicity as measured by cellular ATP levels, up to 100 μM following a 24-h incubation (Table 3 and Supplementary Fig. S2).

Given the potential for pharmacological agents to block either the production or the detection of ROS in whole cells through nonspecific pathways, we also assessed the activity of GSK2795039 in a number of additional assays. First, since the primary pathway for NOX2 stimulation following addition of PMA is through direct activation of protein kinase C (PKC), it was important to demonstrate lack of pharmacological activity on the activity of the PKC enzyme. As shown in Table 1, GSK2795039 did not show any inhibitory activity at PKC beta 2 (PKCB II) up to 25 μM. Second, to confirm that the apparent inhibitory activity in whole cells was not due to either antioxidant activity or a nonspecific direct effect on the L-012 or Oxyburst reagents, we assessed the effect of the compound on the rate of NOX2 substrate utilization by performing oxygen consumption experiments. In neutrophils, NOX assembly and activation trigger the respiratory burst, during which the rate of oxygen consumption is directly related to NOX activity and can be measured using an oximeter. As shown in Figure 3D, GSK2795039 demonstrated a concentration-dependent suppression of oxygen consumption with a maximum effect observed at 20 μM, equivalent to the level of inhibition exhibited by the positive control, 10 μM DPI.

To characterize the activity of GSK2795039 against other NOX isoforms (Table 4), cell-based assays for NOX1,

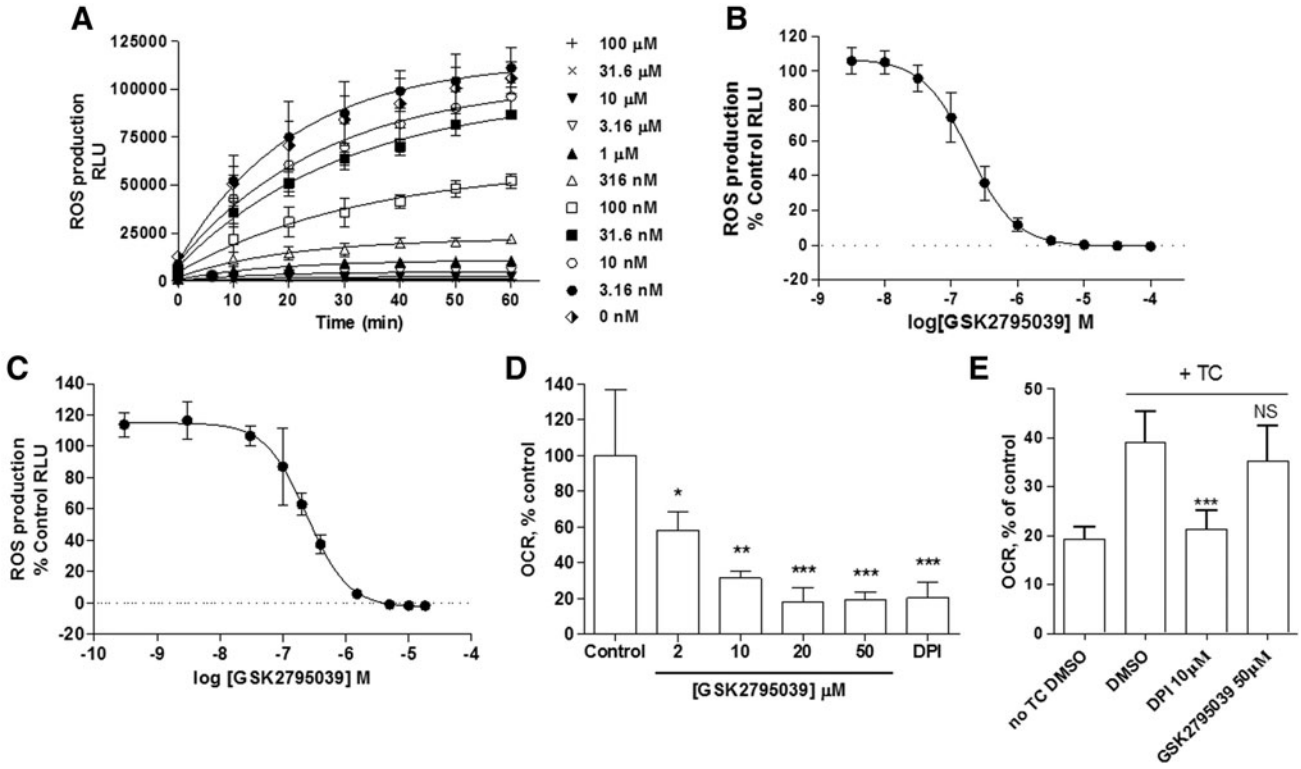

FIG. 3. Effect of GSK2795039 in cell-based ROS detection and oxygen consumption assays. **(A)** Representative kinetic profile of GSK2795039 in differentiated HL60 cellular assays following PMA activation. **(B)** Concentration response curve of GSK2795039 in differentiated HL60 cellular assays following PMA activation. Data were normalized to vehicle-treated control with full inhibitory effect of compound observed at highest concentration tested of 100 μM. **(C)** Concentration response curve of GSK2795039 in human PBMCs following PMA activation. The calculated pIC_{50} was 6.60 ± 0.075. **(D)** Effect of GSK2795039 on the OCR of human PMNs. Raw data were normalized to the mean of the no-compound group. DPI (10 μM) was used as a positive control for NOX2 inhibition. **(E)** Effect of GSK2795039 on the OCR of NOX4 heterologously expressed in T-Rex cells under the control of tetracycline (TC)-dependent promoter after inhibition of mitochondrial respiration. Data are expressed as mean ± standard deviation. Basal respiration levels in tetracycline-induced NOX4-expressing cells before inhibition of mitochondrial respiration were considered as 100%. $*p < 0.05$, $**p < 0.01$, and $***p < 0.001$; NS, nonsignificant. Data are the mean ± standard deviation of replicate experiments ($n = 10$ **[B]**, $n = 4$ **[C]**, and $n = 3$ **[D, E]**). OCR, oxygen consumption rate; PBMCs, peripheral blood mononucleated cells; PMA, phorbol 12-myristate 13-acetate; PMNs, polymorphonuclear leukocytes.

NOX3, NOX4, and NOX5 were used as in Seredenina *et al.* (53). For NOX2, we measured ROS production by differentiated PLB-985 cells (63). All NOX isoforms generated ROS upon activation or stimulation that could be detected using either HRP/Amplex Red or the SOD-inhibitable WST-1 assay. Intriguingly, the two probes generated different profiles of NOX inhibition. In the WST-1 assay, GSK2795039 produced complete inhibition of NOX2 with a pIC_{50} of 5.54 ± 0.25, but was inactive on the other NOX isoforms (up to 100 μM, Table 4). In contrast, inhibitory activity was observed across all isoforms in the HRP/Amplex Red assay. Interestingly, maximal inhibition was ~70% for NOX1, NOX3, NOX4, and NOX5 and H_2O_2 alone, while complete maximal inhibition (>95%) was observed for NOX2 (Table 4). This submaximal activity against some NOX isoforms as well as H_2O_2 alone is most likely due to an off-target effect of GSK2795039 on the HRP/Amplex Red. It is known that reducing agents such as ascorbate interfere with HRP-dependent assays (16). To address the possibility that GSK2795039 has electron donor properties, we performed the colorimetric 2,2-diphenyl-1-picrylhydrazyl (DPPH) assay (34). In the presence of a substance that can donate a hydrogen atom, the violet radical gives rise to its yellow-colored reduced form. Electron donor properties were confirmed for GSK2795039 and *N*-acetylcysteine, but not DPI, with pIC_{50} values of 4.32 ± 0.03 and 4.75 ± 0.36, respectively (Table 3 and Supplementary Fig. S2). Thus, HRP/Amplex Red assay should not be recommended when testing small molecules even with weak reducing activities such as GSK2795039. The selectivity of GSK2795039 for NOX2 over other isoforms was confirmed by measuring oxygen consumption in NOX4-expressing cells. As shown in Figure 3E, DPI fully inhibited NOX4-mediated oxygen consumption, whereas GSK2795039 did not have any effect up to 50 μM.

Enzyme mode of action studies

To understand both the mode of action of GSK2795039 at the enzyme and the apparent selectivity for NOX2 over other NOX isoforms, we explored two potential modes of action: (i) oxidation of cysteine residues in $gp91^{phox}$. Compounds able to oxidize dithiols to form a disulfide complex such as phenylarsine oxide (PAO) (39) and gliotoxin (67) are specific NOX2 inhibitors. They act through a ^{369}CysGlyCys^{371} region

Table 2. Summary of Additional Pharmacology Assays

Assay	*Test compound*	*pIC_{50}*	*% Max effect (100 μM)*
DPPH	GSK2795039	4.32 ± 0.03 (3)	
	DPI	< 4 (3)	
	N-acetylcysteine	4.75 ± 0.36 (3)	
eNOS	GSK2795039	< 4 (1)	50
ATP	L-NMMA	6.7 (2)	
	GSK2795039	< 4 (2)	15

pIC_{50} values for GSK2795039 were generated in the DPPH assay to determine electron accepting properties in comparison with *N*-acetylcysteine and DPI. Inhibitory activity against recombinant eNOS was determined in comparison with the positive control L-NMMA. Cytotoxic effects of GSK2795039 were determined *via* measurement of ATP levels in HEK 293 cells following 24-h compound treatment. Where less than 50% effect was observed (*i.e.*, $pIC_{50} < 4$) at the highest concentration of compound, the % inhibition values are shown. Data are expressed as mean values or mean ± standard deviation (*n*).

DPPH, 2,2-diphenyl-1-picrylhydrazyl; eNOS, endothelial nitric oxide synthase; HEK, human embryonic kidney; L-NMMA, N^G-Monomethyl-L-arginine.

in the NOX2 sequence, which is absent in NOX1, NOX3, NOX4, and NOX5 (33) and is necessary for NOX2 function, probably by mediating the binding of the $p67^{phox}$ subunit (6). When the NOX2 complex is not assembled, the cysteine thiol groups are exposed and $gp91^{phox}$ is more sensitive to thiol-oxidizing compounds. We therefore incubated different concentrations of GSK2795039 and PAO before and after addition of recombinant cytosolic subunits in a semi-recombinant NOX2 assay using PLB-985 cell membranes and WST-1 as the detection reagent.

Table 3. Summary Showing pIC_{50} Values for GSK2795039, DPI, Apocynin, VAS2870, Shionogi 2, Naloxone, ML171, Celastrol, and Suramin in PMA-Activated HL60 Cell-Based NOX2 Assays Using Either L-012 Or Oxyburst Green as the ROS Detection Reagent

	Whole-cell NOX2 assay	
Test compounds	*ROS production L-012*	*ROS production Oxyburst*
GSK2795039	6.74 ± 0.17 (10)	6.73 ± 0.16 (6)
DPI	6.84 ± 0.22 (>10)	6.49 ± 0.18 (>10)
Apocynin	4.32 ± 0.43 (5)[a]	< 4 (5)[b]
VAS2870	6.38 ± 0.03 (4)	< 4 (6)[b]
Shionogi 2	7.04 ± 0.12 (4)	6.73 ± 0.10 (3)
Naloxone	5.38 ± 0.06 (4)	< 4 (6)[b]
ML171	7.03 ± 0.17 (4)	7.44 ± 0.17 (9)
Celastrol	6.06 ± 0.04 (4)	5.55 ± 0.02 (6)
Suramin	< 4 (4)	< 4 (3)

Data are expressed as mean ± standard deviation (*n*). Symbol (<) indicates that compound was inactive and/or showed less than 50% inhibition at top concentrations.

[a]Indicates that compound showed less than 50% inhibition at top concentrations in some replicate experiments, and a value of 4 was used to calculate the population mean.

[b#]Indicates that interference of the test compound with the reagent was observed potentially obscuring a real pharmacological effect.

PMA, phorbol 12-myristate 13-acetate.

Table 4. Summary of pIC_{50} and Maximum Inhibition Values for GSK2795039 in Cellular NOX Isoform Assays Using Either HRP/Amplex Red Or WST-1 as the ROS Detection Reagent

	HRP/Amplex Red		
NOX isoform	*pIC_{50}*	*% Max inhibition*	*WST-1 pIC_{50}*
NOX1	6.30 ± 0.28 (3)	68 ± 2	< 4 (3)
NOX2	6.07 ± 0.24 (3)	98 ± 4	5.54 ± 0.25 (3)
NOX3	6.67 ± 0.34 (3)	62 ± 3	< 4 (3)
NOX4	5.84 ± 0.05 (2)	64 ± 1	< 4 (2)
NOX5	5.88 ± 0.07 (3)	61 ± 3	< 4 (3)
H_2O_2 alone	6.25 ± 0.03 (3)	69 ± 1	NA

The values determined for a control assay using H_2O_2 instead of cells are also shown. Data are expressed as mean ± standard deviation (*n*).

NA, not applicable.

PAO was less active when added afterward, that is, when cysteines were protected (Fig. 4B), while GSK2795039 was similarly active in both conditions (Fig. 4A), suggesting that GSK2795039 does not act through oxidation of thiols. (ii) Competition for the NADPH binding site of NOX2. We considered this possibility based on the fact that the sequences of NADPH binding sites differ significantly among NOX isoforms (Supplementary Fig. S3). Addition of increasing concentrations of NADPH decreased the NOX2 inhibitory potency of GSK2795039. This dependency on the substrate concentration is indicative of a competitive mode of action. The Michaelis–Menten and Lineweaver–Burk plots shown in Figure 4D and E graphically display that similar maximum enzyme velocity (V_{max}) can be reached while the apparent Michaelis constant (K_m) decreases (Supplementary Fig. S4). Increasing concentrations of NADPH did not affect DPI inhibition (Fig. 4C) and both V_{max} and K_m simultaneously decreased with increased concentration of DPI, consistent with an uncompetitive mode of action for NADPH (48) (Supplementary Fig. S4).

Further evidence in support of a competitive mode of action of GSK2795039 was gained by conducting studies in the NADPH depletion assay at a range of NADPH concentrations (25 *μM*–1 m*M*) (Supplementary Fig. S5). For DPI, its inhibitory potency was independent of the NADPH concentration used in the assay, while the measured pIC_{50} values of both suramin and GSK2795039 varied with NADPH concentration. For GSK2795039, the pIC_{50} values were 6.35 ± 0.12 at 25 *μM* NADPH and 5.64 ± 0.05 at 1 m*M* NADPH, consistent with an NADPH competitive mode of action.

Comparison of GSK2795039 with other reported NOX2 inhibitors

The pharmacological profile of GSK2795039 was compared against a number of other reported NOX inhibitors in the various assays described (summarized in Tables 1 and 2). Apocynin, naloxone, Shionogi 2 (21), and VAS2870, all showed some inhibitory effects in whole-cell assays (Table 2). However, they showed little or no inhibitory activity in the semirecombinant cell-free NOX2 assays regardless of whether enzyme activity was measured *via* HRP/Amplex Red,

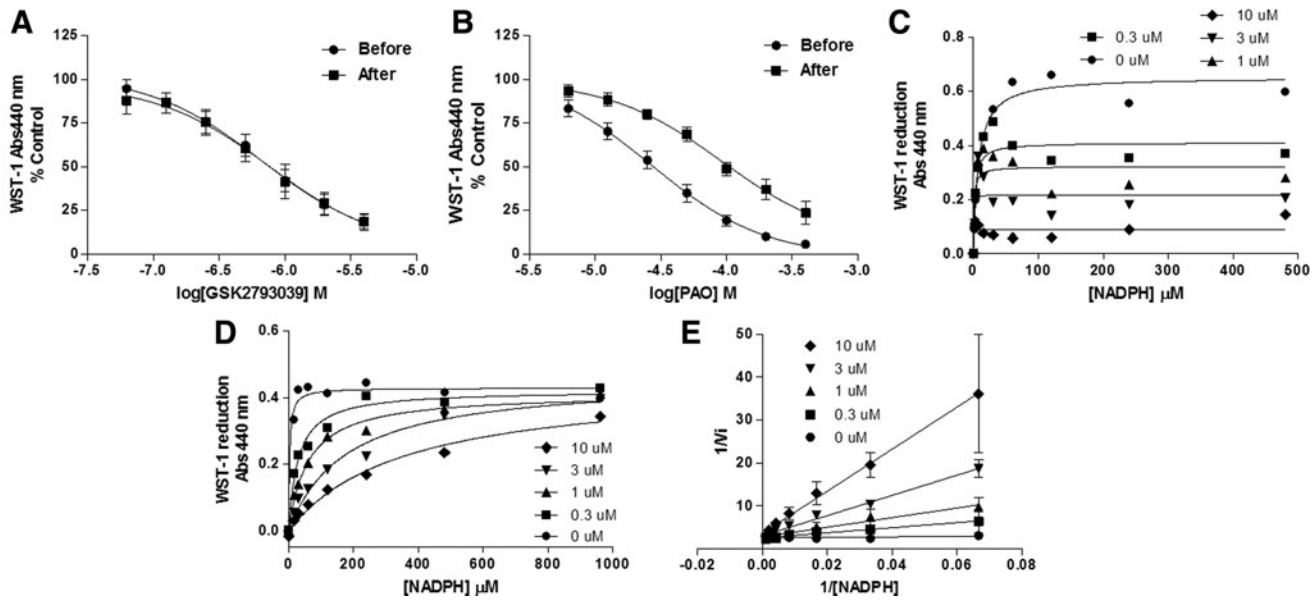

FIG. 4. Mode of action studies of GSK2795039. Concentration response curves of **(A)** GSK2795039 and **(B)** phenylarsine oxide in a semirecombinant NOX2 assay using PLB-985 cell membranes. The compounds were added before or after addition of recombinant subunit proteins. The effect of various concentrations of NADPH was evaluated in a semirecombinant NOX2 assay in the presence of 0.3, 1, 3, and 10 μM of **(C)** DPI and **(D)** GSK2795039. Data are displayed in Michaelis–Menten **(C, D)** and Lineweaver–Burk **(E)** plots and are in agreement with a competitive mode of action for GSK2795039 and uncompetitive for DPI. Graphs in **A–E** are representative curves from $n = 3$ independent experiments.

Oxyburst ROS detection, or *via* NADPH utilization (Table 1). Therefore, the apparent activity in HL60 cells is unlikely to be due to a direct effect on the NOX2 complex. Indeed, for Shionogi 2, it is likely that inhibition of PKCB II (pIC_{50} 7.6 ± 0.27) is responsible for the apparent activity in HL60 cells. However, this mechanism of action cannot account for the inhibitory activity of naloxone, VAS2870, and apocynin since they were not found to inhibit PKCB II. Suramin, DPI, and celastrol inhibited ROS production and NADPH utilization in the recombinant NOX2 enzyme system in Amplex Red/HRP, Oxyburst, and NADPH assays (Table 1), but suramin was inactive in whole cells (Table 2), perhaps due to lack of cell membrane penetration (60). Celastrol showed inhibitory activity in cell-free NOX2 assays as well as in HL60 cells. DPI, consistent with its known mode of action, that is, inhibition of most flavoproteins, also showed consistent inhibitory activity across all five NOX2 assays and the xanthine oxidase assay. ML171 showed apparent inhibition in both HL60 cell-based assay readouts (Table 2) and in the semirecombinant cell-free system using HRP/Amplex Red and Oxyburst as the detection methods (Table 1), but did not show any effect in the NADPH depletion assay. This is likely due to assay interference as previously reported for this compound (53).

Systemic administration of GSK2795039 in mice inhibits the NOX2 enzyme in vivo

The pharmacokinetic properties (summarized in Table 5) of GSK2795039 were determined in rat and mouse. Following intravenous (i.v.) infusion, GSK2795039 had a moderate-to-high clearance rate in rat and mouse of 54 and 95 ml/min/kg with half lives of 2 and 0.2 h, respectively. GSK2795039 was moderately brain penetrant with brain: blood ratios of 0.83 and 0.49 in rat and mouse, respectively, after intraperitoneal (i.p.) administration. In rat, following oral administration (p.o.) at 3 mg/kg, the oral bioavailability was poor (3%) with a peak blood concentration (C_{max}) of only 46 nM in blood. In mouse, oral bioavailability was higher and varied between 10% and 54% when dosed at 5 and 100 mg/kg, respectively, with associated blood C_{max} values of 0.2 and 11 μM.

TABLE 5. SUMMARY OF GSK2795039 PHARMACOKINETIC PROPERTIES IN RAT AND MOUSE

Parameter	*Units*	*Rat*	*Mouse*
Blood clearance (Clb)	ml/min/kg	54	95
Half life ($t_{1/2}$) i.v.	h	2	0.2
Volume of distribution (V_{ss})	l/kg	9.3	2.5
Brain:blood ratio	Median ratio	0.83	0.49
Oral C_{max}	μM	0.046 (3)	0.2 (5) 11.5 (100)
Oral T_{max}	h	0.5 (3)	0.5 (5) 0.5 (100)
Oral bioavailability (F_{po})	%	3 (3)	10 (5) 54 (100)

Blood clearance, half-life, volume of distribution, oral C_{max} and T_{max} were estimated using a noncompartmental model. The oral bioavailability was estimated using results obtained from intravenous (1 mg/kg) and oral profile studies (3, 5 or 100 mg/kg as shown in parenthesis). C_{max} and T_{max} values were determined following oral dosing at the doses (mg/kg) indicated in parenthesis. The brain:blood ratios (median value) were determined at 1 hour following intraperitoneal injection at 100 mg/kg.

C_{max}, peak blood concentration; T_{max}, time to reach C_{max}.

GSK2795039 was further evaluated in mice to determine whether systemic administration inhibited the NOX2 enzyme in different tissues *in vivo*. NOX2 activity was assessed following the induction of inflammation in the hind paw of mice *via* injection of complete Freund's adjuvant (CFA), which is known to trigger neutrophil migration to the paw with subsequent localized NOX2-dependent respiratory burst (43, 50, 63). Enzyme activity was monitored 24 h after CFA injection into the plantar surface *via* systemic administration of L-012 (25 mg/kg). Activated L-012 reagent was detected by whole animal luminescence imaging. As shown in Figure 5A, the L-012-derived chemiluminescence in the inflamed paw reached its maximum at ~10 min after L-012 injection and decreased gradually over the next 15 min, presumably due to clearance of L-012 from the circulation. In gp91^{phox}-deficient mice, the L-012 signal in the inflamed paw was nearly abolished compared with wild-type mice (Fig. 5A). This suggests that NOX2 is the main enzyme responsible for the production of superoxide in the inflamed paw.

Following i.p. administration, GSK2795039 dose-dependently inhibited the L-012 signal in the inflamed paw with ~50% inhibition observed at 2 mg/kg and almost complete suppression of enzyme activity at 100 mg/kg compared with vehicle-treated animals (Fig. 5B). Following a single 100 mg/kg i.p. dose, complete inhibition of enzyme activity in the paw was observed at 1 and 2 h postdose (Fig. 5C). Significant inhibition of enzyme activity was still observed up to 6 h postdose (Fig. 5C), while 24 h postdose enzyme activity was similar to vehicle-treated animals. The concentration of GSK2795039 in blood measured at 1 h postdose was 7.9 μM and was below the limit of quantification at 24 h postdose. To compare other NOX2 inhibitors with GSK2795039, we also evaluated apocynin (100 mg/kg, i.p.), celastrol (100 mg/kg, p.o.), and naloxone (50 mg/kg, subcutaneous [s.c.]) in the paw inflammation assay. As shown in Figure 5D, no reduction in NOX2 enzyme activity was observed following treatment with any of these compounds.

GSK2795039 is active in a mouse model of acute pancreatitis

To evaluate whether the *in vivo* inhibition of NOX2 by GSK2795039 also resulted in biological effects consistent with the known *in vivo* function of the NOX2 enzyme, we

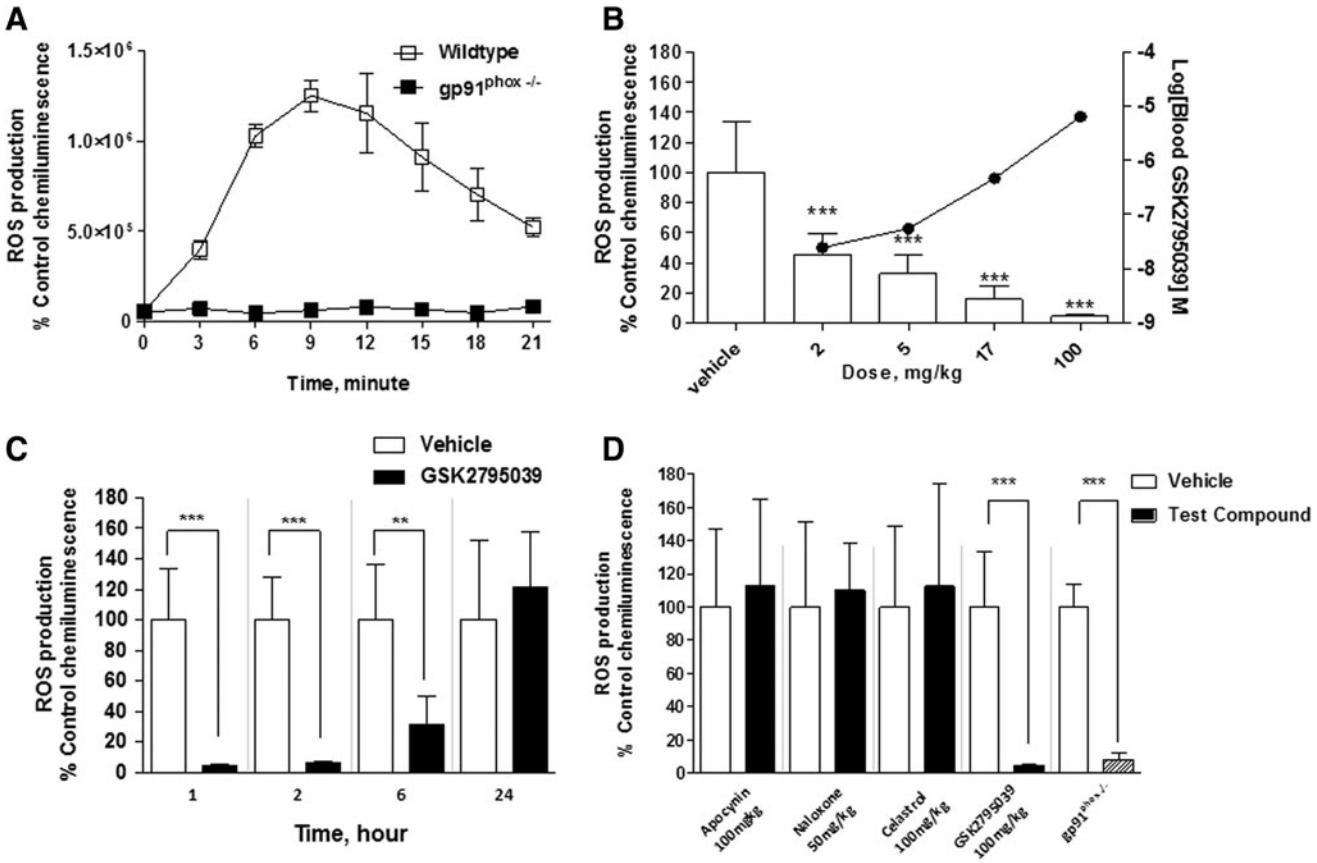

FIG. 5. Effect of GSK2795039 and reported NOX inhibitors on NOX2 enzyme activity *in vivo*. **(A)** The chemiluminescent signal generated in the inflamed paw of wild-type and gp91$^{phox-/-}$ mice following the injection of L-012. **(B)** Effect of GSK2795039 on the chemiluminescent signal in the inflamed paw and compound blood concentration at 60 min after i.p. dosing. GSK2795039 achieved ~50% and 95% inhibition of the L-012 chemiluminescent signal at 2 and 100 mg/kg, respectively. **(C)** Effect of 100 mg/kg GSK2795039 at 1, 2, 6, and 24 h after dosing. **(D)** Effect of apocynin (30 min after dosing, 100 mg/kg i.p.), naloxone (15 min after dosing, 50 mg/kg s.c.), celastrol (1 h after dosing, 100 mg/kg p.o.), and GSK2795039 (1 h after dosing, 100 mg/kg i.p.). A similar level of L-012 chemiluminescent signal was observed in gp91$^{phox-/-}$ mice compared with GSK2795039-treated mice. Data are expressed as mean ± standard deviation. $^{**}p < 0.01$ and $^{***}p < 0.001$. i.p., intraperitoneal; p.o., oral administration; s.c., subcutaneous.

assessed the effect of GSK2795039 in the cerulein model of acute pancreatitis in mice. We chose this model because gp91^{phox} knockout mice, but not myeloperoxidase-deficient mice, were shown to be protected (26). GSK2795039 (100 mg/kg) was administered twice *via* i.p. injection; the initial dose given 1 h before the first of 6 hourly injections of cerulein (50 μg/kg), the second dose given 4 h later (*i.e.*, at the time of the fourth cerulein injection). The mice were sacrificed 1 h after the last injection of cerulein and levels of serum amylase, the marker for pancreatic cell necrosis, were quantified. As shown in Figure 6, GSK2795039 caused $\sim$50% reduction in the level of serum amylase activity similar to what was previously reported for gp91^{phox} knockout mice (26).

Discussion

In this study, we describe the pharmacological profile of GSK2795039, the first small molecule to demonstrate inhibition of the NOX2 enzyme following systemic administration *in vivo*. To enable the discovery of GSK2795039, several assays were developed to measure NOX2 activity in different biological systems using mechanistically diverse detection methodologies. To unequivocally confirm blockade of NOX2 enzyme activity in a biological system, it is critical to demonstrate that a compound inhibits not only the catalytic formation of ROS, as measured using multiple ROS detection reagents, but that it also blocks the utilization of substrate in both semirecombinant cell-free enzyme and whole-cell-based systems. As such, we have compiled a pharmacology data set sufficient to claim that GSK2795039 is a true NOX2 inhibitor.

In the semirecombinant system, GSK2795039 is a potent inhibitor of NOX2-dependent ROS production (as measured using WST-1, HRP/Amplex Red, and Oxyburst detection methods) and NADPH utilization. In HL60 cells, human PBMCs, and polymorphonuclear leukocytes (PMNs), it is a potent inhibitor of NOX2-dependent ROS production as measured by L-012 chemiluminescence, HRP/Amplex Red fluorescence, Oxyburst fluorescence, and WST-1 absorbance. In PMNs following PMA stimulation, it blocks utilization of oxygen, the substrate of the reaction catalyzed by NOX2. In neutrophils, activated NOX2 contributes >95% of the total oxygen consumption (11) as evidenced by oxygen consumption measurements of neutrophils from chronic granulomatous patients who have genetic loss of function of NOX2 (9, 51).

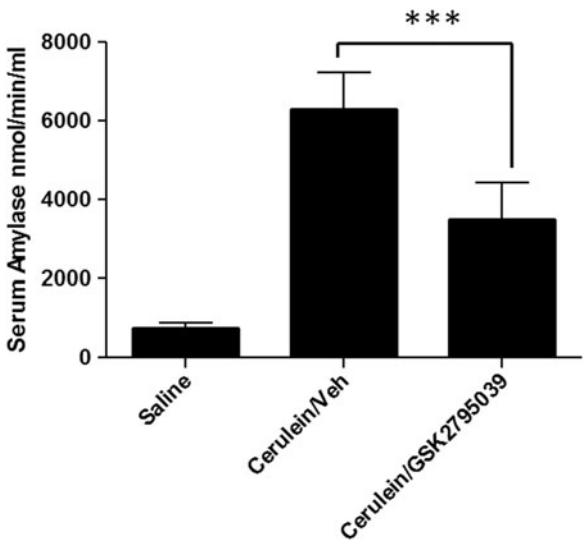

FIG. 6. Effect of GSK2795039 in the cerulein model of acute pancreatitis. C57BL6 mice were treated twice with vehicle ($n=7$) or 100 mg/kg GSK2795039 ($n=7$) i.p. The first dose was given 1 h before 6 hourly i.p. injections of cerulein (50 μg/kg) and the second dose given 4 h later. The control group ($n=2$) was administered with saline instead of cerulein. Serum amylase levels were quantified in blood samples collected 1 h after the last cerulein injection. Data are expressed as mean $\pm$ SEM. ***$p<0.001$.

The NOX activity assays measuring substrate utilization, that is, oxygen consumption in whole cells and NADPH depletion in cell-free assays, are of utmost importance in defining GSK2795039 as a direct inhibitor of NOX2. In terms of orthogonal assays, GSK2795039 is not cytotoxic and does not inhibit PKC nor xanthine oxidase at concentrations efficacious for NOX2 inhibition.

The rationale for using such a range of assays was to address the difficulties associated with the use of any one assay in isolation, in particular with regard to the potential nonspecific effects of test compounds. This is illustrated simply by the profile of the Shionogi 2 compound, which initially appeared to be a potent inhibitor of ROS production in HL60 cells, but was inactive in the cell-free semirecombinant NOX2 enzyme assay. It acts in fact as a potent PKC inhibitor, thereby blocking the PKC-dependent translocation of NOX2 subunits upon PMA stimulation.

Our study is also representative of the fact that ROS detection assays using fluorescent or luminescent ROS sensitive reagents are susceptible to interference and prone to detecting nonspecific effects of compounds [reviewed in Maghzal *et al.* (42)]. It is only by using a variety of assays that we demonstrated the selectivity of GSK2795039 for NOX2. A superficial interpretation of the results of the HRP/Amplex Red detection, for example, would suggest apparent nonselective pharmacological activity across all NOX isoforms. As the compound showed inhibition of HRP/Amplex Red when activated by H_2O_2 alone (Table 4), a nonspecific effect of GSK2795039 on the HRP/Amplex Red was most likely. Although we did not address the chemistry of the interaction between GSK2795039, Amplex Red, and HRP, it is possible that adding a small molecule with one-electron reducing capacity diverts compound I of HRP (or other heme-containing peroxidases) from its normal cycle (16, 19). The fact that GSK2795039 is inactive in NOX4-dependent oxygen consumption as well as in the WST-1 assay for NOX1, NOX3, NOX4, and NOX5 confirms GSK2795039 selectivity for NOX2. However, this stresses the fact that future studies using GSK2795039 should avoid the use of HRP/Amplex Red assay and that extreme care should be taken in the interpretation of results when small molecules are used in peroxidase-dependent ROS detection methods (69).

In addition to the *in vitro* characterization presented here, we have shown that GSK2795039 is orally available and can be measured in the blood and central nervous system, suggesting that it can cross the blood–brain barrier. It fully inhibits NOX2 enzyme activity *in vivo* following systemic dosing in mice. Importantly, the level of inhibition achieved at the highest dose was complete and equivalent to that

observed in gp91^{phox}-deficient mice as measured by *in vivo* L-012 chemiluminescence. The potent activity *in vivo* confirms the bioavailability of the compound and the validity of the cell-free and cell-based assays used in defining NOX2 activity, despite the potential flaws inherent in these assays. For example, in the cell-free semirecombinant assay, the use of cell membranes from BHK cells overexpressing gp91^{phox}/p22^{phox} or the use of arachidonic acid as the mode of enzyme activation may have generated an enzyme system that was not representative of the enzyme composition or activation mechanism, respectively, *in vivo*. Second, in the cell-based assay, we only evaluated compounds for activity against the enzyme when activated by PMA, which may not accurately recapitulate the dynamics of enzyme activation *in vivo*. In the paw inflammation paradigm, we can assume that the NOX2 enzyme is assembled and activated in a more physiologically relevant way, and as such, it is an important confirmation that GSK2795039 is active at the endogenous enzyme in this *in vivo* biological context. Importantly, the paw inflammation studies also demonstrate that inhibition of NOX2 by GSK2795039 is reversible since 24 h after administration, when the levels of compound in blood were undetectable, ROS production induced by CFA was similar to that in vehicle-treated animals.

The paw inflammation model enabled us to fully characterize the relationship between dose, blood exposure, and NOX2 enzyme inhibition *in vivo* over time, a critical data set required to enable the appropriate design and interpretation of studies aimed at evaluating the effect of GSK2795039 in more complex *in vivo* systems. The other reported NOX2 inhibitors, celastrol, naloxone, and apocynin, did not demonstrate significant inhibition of ROS production in the paw inflammation model. As such, this is the first direct demonstration of pharmacological inhibition of NOX2 *in vivo* with a small molecule inhibitor.

We have also used an acute pancreatitis model to show that GSK2795039 has *in vivo* physiological effects consistent with NOX2 inhibition since GSK2795039 recapitulates the effect of genetic ablation of gp91^{phox} in the same mouse model. We also observed that GSK2795039 (100 mg/kg) was well tolerated in rodents, with no obvious adverse effects following 5 days of twice daily dosing *via* the p.o. or s.c. dose routes (data not shown), and is therefore a suitable tool molecule to further characterize NOX2 biology.

Mechanistic evaluation in the cell-free NOX2 semirecombinant assay using WST-1 revealed a competitive inhibition of GSK2795039 toward NADPH and excluded a potential action on intracellular cysteines, a known inhibitory mode of action specific for NOX2 (6). This finding was confirmed when NADPH depletion was used as readout. This is an important finding because it indicates that NADPH binding sites are sufficiently divergent among NOX isoforms to allow isoform-specific inhibition. Future structural analysis of the gp91^{phox} NADPH binding site by cocrystallization with GSK2795039 may reveal a specific pocket.

Among other NOX inhibitors tested in this study, only DPI, celastrol, and suramin showed inhibition across the cell-free assays independently of assay format, in agreement with previous reports suggesting that DPI is an irreversible inhibitor of NOX2 (14), that celastrol inhibits NOX2 directly and *via* binding to the p47^{phox} subunit (30), and that suramin also acts *via* binding to the NADPH binding site (21). While DPI and celastrol also demonstrated inhibitory activity in the cell-based assays, suramin was not active, perhaps due to lack of cell penetrance as has previously been suggested (60). The other reported NOX inhibitors, apocynin, naloxone, Shionogi 2, VAS2870, and ML171, showed similar activity in the cell-based assays used here to the previously described whole-cell systems (3, 12, 23, 31), although the potency of apocynin was rather weak. However, they were mostly inactive in the cell-free assays with the exception of ML171, which showed activity in the HRP/Amplex Red and Oxyburst assays, but not the NADPH depletion assay, and Shionogi 2, which showed weak activity only in the Oxyburst assay. Notwithstanding their potential therapeutic or pharmacological value, this highlights the fact that none of these compounds act directly on the NOX2 complex, but rather have indirect modes of action on NOX2-derived ROS. For example, the reported pharmacology of VAS2870 is complex with activity in cell-free assays only observed if added before addition of sodium dodecyl sulfate (SDS) to induce enzyme assembly (2). In the cell-free assay used here, the enzyme components were preassembled and activated with arachidonic acid before addition of compound, followed by NADPH. Therefore, the assay may not have been optimal to detect its activity if the mode of action is *via* inhibition of subunit assembly. The reported pharmacology of naloxone at NOX2 is also complex as it is proposed to bind to the gp91^{phox} subunit of NOX2 and inhibit enzyme activity by modulation of p47^{phox} subunit translocation (65). The method for the cell-free assay used here differs from what was previously used to demonstrate naloxone activity because we used a fully recombinant enzyme activated with arachidonic acid, whereas the assay reported by Wang *et al.* (65) used PMA-activated neutrophil membranes in a semirecombinant system. In the case of Shionogi 2, however, we found that it is a potent PKC inhibitor, consistent with previous reports (21), and this likely explains its apparent inhibitory activity in HL60 cells. For ML171, no mode of action at the NOX2 enzyme has been described, but it has recently been shown that it is most likely not an NOX inhibitor (53).

While variations in the configuration of the *in vitro* assays may explain apparent pharmacological differences between GSK2795039 and other reported NOX inhibitors, the paw inflammation assay clearly highlights that GSK2795039 is distinct in terms of its *in vivo* pharmacological activity. The doses of apocynin (100 mg/kg), naloxone (50 mg/kg), and celastrol (100 mg/kg) used here were selected on the basis of doses reported to be efficacious in various disease models (13, 17, 35, 40, 55). None of these three compounds showed NOX2 inhibition in the paw inflammation model. There are a number of potential explanations for the observed lack of activity. First, it is possible that the mechanism of NOX2 enzyme activation differs between different *in vivo* biological systems, which may therefore have different sensitivities to inhibitors with alternative modes of action at the enzyme. It is also possible that the levels of tissue exposure, specifically in the inflamed paw, were not sufficient to elicit a significant effect at the enzyme. Alternatively, it is possible that the pharmacology shown at least in the cell-based HL60 assay does not translate to the *in vivo* system. Either way, our results raise the possibility that the reported biological effects of these molecules in disease models may be driven by additional pharmacology beyond NOX2. We did not evaluate

VAS2870 in the paw inflammation model because we found that the compound was rapidly degraded in blood and hence unsuitable for *in vivo* experiments, nor did we test suramin due to its lack of cell penetration. While we have not profiled all the reported NOX inhibitors, for example, fulvene-5 (8) and imipramine (44) have also been reported to inhibit NOX enzymes, GSK2795039 is the only NOX inhibitor tested here that demonstrates a convincing *in vitro* pharmacological profile combined with *in vivo* pharmacological activity at the NOX2 enzyme.

Only celastrol and DPI were active in all assays and may be *bona fide* NOX inhibitors *in vitro*; however, they may not be suitable tools to test NOX enzyme function *in vivo*. As we have shown, celastrol does not appear to inhibit NOX2 *in vivo* at the doses tested here. DPI, as well as being a nonspecific irreversible inhibitor of flavin-dependent enzymes, is limited in terms of its *in vivo* utility by its high toxicity in rodents ($LD_{50} < 10$ mg/kg) (20, 49). Consistent with the observed NOX2 enzyme inhibition following systemic dosing, we have also demonstrated that GSK2795039 has the same biological effect as $gp91^{phox}$ gene ablation in a rodent model of acute pancreatitis (26).

In summary, we report here the discovery of a novel small molecule NOX2 inhibitor, GSK2795039, which inhibits enzyme activity in both cell-free and whole-cell systems. Importantly, GSK2795039 was bioavailable after systemic administration and showed *in vivo* target engagement in peripheral tissues, thus supporting the utility of GSK2795039 as a tool NOX2 inhibitor to further evaluate the biology of the NOX2 enzyme and the therapeutic potential of NOX2 inhibitors in acute and chronic inflammatory diseases, such as pulmonary inflammation (29) and neurodegenerative diseases (46), where genetic deletion of NOX2 has been shown to be protective.

Materials and Methods

Reagents

GSK2795039, *N*-(1-Isopropyl-3-(1-methylindolin-6-yl)-1*H*-pyrrolo[2,3-*b*]pyridin-4-yl)-1-methyl-1*H*-pyrazole-3-sulfonamide, was synthesized by the Neural Pathways Discovery Performance Unit, GlaxoSmithKline (Biopolis, Singapore). All purified recombinant cell-free NOX subunits ($p47^{phox}$, $p67^{phox}$, and Rac2), BacMam viruses ($gp91^{phox}$ and $p22^{phox}$), and DNA plasmids harboring NOX cDNAs (Rac1 and $p22^{phox}$) were generated by GlaxoSmithKline Platform Technology & Sciences (Stevenage, United Kingdom). NOX isoform-specific cells were generated by the University of Geneva (Geneva, Switzerland); for detailed description, see Seredenina *et al*. (53) and references therein. The human biological samples, PBMCs, were used in accordance with the terms of approval by the Human Biological Sample Users committee, GlaxoSmithKline. PMNs were used in accordance with the terms of the Ethics Commission of the Research on Human Beings of the Geneva University Hospitals and informed consents. Sources of other reagents are indicated where appropriate.

Animals

Male Sprague-Dawley (SD) rats (Charles River Laboratories, Inc., and Animal Resources Centre), C57BL6/J mice (Biological Resource Centre), and $gp91^{phox}$ knockout mice (Jackson Laboratories) were used in this study. Animals were housed in groups of five at controlled temperature (20°C ± 1°C) and humidity (40% ± 2%) with a 12-h light/12-h dark cycle and allowed *ad libitum* access to water and food. All studies were conducted in accordance with the GlaxoSmithKline Policy on the Care, Welfare, and Treatment of Laboratory Animals. Animal experiment protocols were reviewed and approved by the Singapore National Advisory Committee at the Biological Resource Centre, Biopolis.

Cell-free recombinant NOX2 enzyme assays (BHK cell membranes)

Cell-free NOX2 enzyme preparations were prepared using membranes from either transduced BHK/AC9 cells (European Collection of Cell Cultures) (18) or from differentiated PLB-985 myeloid cells. To generate the BHK cell membranes coexpressing human $gp91^{phox}$ and $p22^{phox}$, full-length cDNAs were cloned into BacMam vectors. BacMam viruses were prepared from Sf9 cells as previously described and used to transduce BHK cells (18). Homogenized cells expressing $gp91^{phox}$/$p22^{phox}$ were collected by high-speed centrifugation, resuspended in 10% sucrose buffer, then layered on top of a 40% sucrose buffer solution. Following centrifugation at 28,500 rpm for 60 min, the interface layer was collected and further centrifuged to isolate cell membranes. Cytosolic proteins used to reconstitute NOX2 enzyme in BHK cells were full-length N-terminal His-tagged human $p47^{phox}$ and human $p67^{phox}$, and human Rac2 proteins were expressed individually in Sf9 cells *via* baculovirus transduction and purified using Ni-NTA affinity resin (Qiagen). Fractions were further purified by size exclusion chromatography on Superdex 200 (GE Healthcare Life Sciences).

The potency of test compounds to inhibit ROS production by the reconstituted recombinant NOX2 enzyme was measured using either HRP/Amplex Red or Oxyburst Green (Life Technologies) detection reagents. Enzyme activity was also measured by quantification of NADPH utilization. For HRP/Amplex Red-mediated ROS detection, the activated NOX2 enzyme mixture (20 n*M* Rac2, 100 n*M* $p47^{phox}$, 150 n*M* $p67^{phox}$, 0.0046 μg/μl $gp91^{phox}$-$p22^{phox}$-BHK membranes, and 20 μ*M* arachidonic acid) was prepared in assay buffer (10 μ*M* FAD, 1 m*M* EGTA, 4 m*M* $MgCl_2$, 1 μ*M* GTPγS in 50 m*M* KPO_4 at pH 7) supplemented with 2 U/ml HRP. Test compounds diluted in assay buffer were incubated with the enzyme mixture for 15 min at room temperature before addition of the enzyme substrate and detection mix (50 μ*M* NADPH, 25 U/ml catalase beads, and 20 μ*M* Amplex Red final concentrations in assay buffer) to yield a final assay volume of 25 μl and dimethyl sulfoxide (DMSO) concentration of 1%. At 5 min after addition of substrate, fluorescence was detected at $\lambda_{Ex}/\lambda_{Em} = 560$ nm/590 nm using a BioTek spectrophotometer. For Oxyburst Green detection of ROS, the assay was run using the same conditions as for the HRP/Amplex Red assay, except that 250 μg/ml Oxyburst Green was used in place of Amplex Red in the enzyme substrate mix, and HRP was omitted. The enzyme reaction was incubated for 90 min. Fluorescence was detected at $\lambda_{Ex}/\lambda_{Em} = 485$ n*M*/530 n*M* at $t = 0$ and $t = 90$ min using a BioTek spectrophotometer to calculate the enzyme rate over 90 min. Test compound pIC_{50} values for both assays were determined

from concentration response curves using a four-parameter logistic curve fitting model.

To measure NADPH utilization (*i.e.*, substrate depletion), test compounds were incubated with the same NOX2 enzyme mixture for 25 min at room temperature. NADPH (50 μM) was added and absorbance measured at 340 nm using a microplate spectrophotometer (BioTek) at 10-min intervals to determine the rate of NADPH utilization [$(Abs_{t=60} - Abs_{t=0})$/60 min]. The pIC_{50} values were calculated from concentration response curves using a four-parameter logistic curve fitting model. To conduct enzyme mode of action studies in the NADPH depletion format, assay conditions were exactly as above, except that NADPH concentrations were varied between 25 and 1000 μM.

Cell-free recombinant NOX2 enzyme assays (PLB-985 cell membranes)

PLB-985 myeloid cells were cultured in RPMI medium supplemented with fetal bovine serum (FBS; 10%), penicillin (100 U/ml), and streptomycin (100 μg/ml) and grown at 37°C in air with 5% CO_2. The cells were differentiated into granulocyte-like cells by the addition of DMSO (1.25%) to the medium for 3–5 days. To prepare NOX2-containing membranes, differentiated PLB-985 cells from wild-type (64) and NOX2 knockout (68) were used. Approximately 10^7 cells were homogenized in 1.5 ml of a sonication buffer containing phosphate-buffered saline (PBS) (0.1×), sucrose (11%), NaCl (120 mM), and EGTA (1 mM) supplemented with protease inhibitors (Complete Mini; Roche) and sonicated twice for 45 s (level 4, Branson Sonifier 250). Cell debris were removed by 10-min centrifugation at 800 *g*. The supernatant was laid on a sucrose gradient consisting of a bottom layer of 1.5 ml sucrose (40%) and an upper layer of 1.5 ml sucrose (17%). Ultracentrifugation was performed at 150,000 *g* in an SW60 rotor for 30 min at 4°C. Following separation, the upper cytosolic fraction was discarded and the cloudy membrane fraction was kept, protein content was measured using the standard Bradford procedure, and was stored in small aliquots at −80°C.

Measurement of ROS generation by NOX2-containing membranes was performed as previously described (58, 53) with slight modification such as the use of WST-1 absorbance or Oxyburst Green fluorescence as readouts. Briefly, 1 μl of various concentrations of compounds dissolved in DMSO was incubated in 80 μl of a mix containing NOX2 membranes (1 μg of protein), 0.5 μg p67Np47N chimeric protein (a fusion of the N-termini of human $p67^{phox}$ [residues 1–210] and p47phox [residues 1–286]), 0.4 μg Rac1Q61L, 0.025 μM FAD, 90 μM SDS, and 1 mM WST-1 or 250 μg/ml Oxyburst Green assay in PBS. After 5 min at room temperature, the reaction was initiated by addition of 20 μl NADPH (final 60 μM). For WST-1, absorbance was immediately measured at 440 nm in a FlexStation® 3 Multimode Microplate Reader (Molecular Devices) at 37°C for 30–60 min. Oxyburst Green fluorescence was measured in a BMG Fluostar Optima Microplate Reader with excitation 485 nm and emission 530 nm after 90 min.

For enzyme mode of action studies, the enzyme assay was initiated by the addition of different concentrations of NADPH (0–960 μM). ROS generation was measured using WST-1 over the first 30 min to calculate an enzyme rate. Michaelis–Menten and Lineweaver–Burk analyses were performed in GraphPad Prism 6.

For the evaluation of potential thiol-oxidizing activity of test compounds, cell membranes and recombinant proteins were mixed with compounds immediately or after 5 min of preincubation. After another 5 min, 60 μM NADPH was added. WST-1 absorbance was measured after 1 h. Test compound pIC_{50} values for both assays were determined from concentration response curves using a four-parameter logistic curve fitting model.

Xanthine oxidase, eNOS, and PKCB II assay

Test compounds were incubated with 5 mU/ml bovine-derived xanthine oxidase (Life Technologies) for 15 min at room temperature, followed by the addition of substrate and detection mix (final concentrations of 0.2 U/ml HRP, 5 μM hypoxanthine, and 50 μM Amplex Red) in 18 μl assay volume. Fluorescence ($\lambda_{Ex}/\lambda_{Em}$ = 535 nm/590 nm) was detected every minute using an Envision spectrophotometer (PerkinElmer, Inc.) for 10 min to determine the enzyme rate. The pIC_{50} values for test compounds were calculated from concentration response curves using a four-parameter logistic curve fitting model.

The activity of test compounds to inhibit recombinant human PKCB II (ProQinase) was determined using the IMAP Screening Express and Progressive Binding Bead System (Molecular Devices) with a fluorescein-labeled 5-FAM-KRREILSRRPSYR-NH2 peptide (FAM; Molecular Devices). Fluorescence polarization measurements were taken at $\lambda_{Ex}/\lambda_{Em}$ = 485 nm/535 nm with a 505 nm dichroic mirror using an Acquest plate reader (Molecular Devices). The pIC_{50} values for test compounds were calculated from concentration response curves using a four-parameter logistic curve fitting model.

The eNOS assay was run at CEREP.

DPPH assay

For the DPPH radical scavenging assay, 2 μl of serial dilutions of compounds in DMSO was mixed with 180 μl of DPPH in methanol (40 μg/ml) in each well of a 96-well plate. The plate was kept in the dark for 15 min, after which the absorbance of the solution was measured at 540 nm in a FlexStation 3 microplate reader. *N*-acetylcysteine and DPI were used as positive and negative controls, respectively.

Cellular ATP assay

Potential cytotoxic effects of test compounds were evaluated in HEK 293 cells. Cells (20,000 cells/well) were cultured for 24 h in the presence or absence of test compound. Cells were then washed and ATP levels quantified using a Cell Titre-Glo assay kit (Promega).

NOX2 HL60 and PBMC-based assays

The activity of test compounds to inhibit endogenous NOX2 in whole cells was performed using differentiated HL60 cells (American Type Culture Collection) and human PBMCs. HL60 cells were differentiated into neutrophil-like cells by culturing in medium containing Iscove's modified Dulbecco's media (Life Technologies), 20% heat-inactivated FBS (Life Technologies), and 1.3% DMSO for 6 days. Compounds were preincubated with 10,000 cells in Hank's balanced salt solution (HBSS) containing 0.1% glucose and

0.01% 3-[(3-cholamidopropyl)dimethylammonio]-1-propanesulfonate (CHAPS), then stimulated with 12 n*M* PMA. Production of ROS was monitored with 125 μM L-012 (Wako Pure Chemical Industries Ltd.) in a 50 μl final assay volume every 10 min up to 60 min using a Microbeta Trilux luminescence counter (PerkinElmer, Inc.). For the calculation of pIC_{50} values, the luminescence signal at 60 min was used and concentration response curves were analyzed using a four-parameter logistic curve fitting model. An alternative ROS detection assay was established in HL60 cells using Oxyburst Green. This assay used the same conditions as for the L-012 assay, except for the following changes: 1 μg/ml Oxyburst was used in place of L-012; 50,000 cells per well; 40 n*M* PMA; and 120-min incubation time. Fluorescence was detected at the end of the incubation at $\lambda_{Ex}/\lambda_{Em} = 485$ nm/530 nm using a BioTek spectrophotometer. For the calculation of pIC_{50} values, concentration response curves were analyzed using a four-parameter logistic curve fitting model.

Human PBMCs were isolated from the blood of healthy donors (StemEasy) using Lymphoprep density gradient medium (Axis-Shield Plc.) and resuspended at 5×10^5 cells/ml in HBSS buffer. Cells (25,000) were incubated with test compound, 400 μM L-012, and 0.01% CHAPS for 15 min at room temperature. PMA (127 n*M*) was added to produce an assay volume of 200 μl, and chemiluminescence was detected 30 min later using an Infinite 1000 spectrophotometer (Tecan). The pIC_{50} values for test compounds were calculated from concentration response curves using a four-parameter logistic curve fitting model.

NOX isoform cell-based assays

To compare the pharmacology of test compounds across the NOX isoforms, NOX1–5-expressing cells were generated as previously described. Briefly, NOX1-expressing cells were generated by transduction of Chinese hamster ovary cells with human NOX1, NOXO1, NOXA1, and $p22^{phox}$ (30); the NOX3-expressing tetracycline-inducible HEK T-Rex cell line was generated using NOX3, NOXO1, NOXA1, and $p22^{phox}$ (63); and NOX4 and NOX5-expressing cell lines were generated as previously described (54). PLB-985 cells, differentiated into granulocyte-like cells by the addition of DMSO (1.25%) to the medium for 72 h, were used for the NOX2 isoform (64).

ROS were measured using HRP-dependent Amplex Red (Life Technologies) or a colorimetric probe, WST-1 (Dojindo Molecular Technologies, Inc.). At least three independent experiments were performed for all measurements. For Amplex Red/HRP assay, cells were preincubated with the test compound for 10 min at room temperature in PerkinElmer black 96-well microplates at 50,000 cells per well, after which the reaction mixture was added to a final concentration of 25 μM of Amplex Red and 0.05 U/ml of HRP in HBSS. NOX enzymes were activated *via* 100 n*M* PMA (NOX1, NOX2), 1 μg/ml tetracycline for 24-h activation of inducible genes (NOX3, NOX4), and 1 μM Ca^{2+} ionophore ionomycin (NOX5). Fluorescence measurements were then performed using a FluoSTAR OPTIMA plate reader (BMG Labtech) every minute for 60 min at 37°C with $\lambda_{Ex}/\lambda_{Em} = 570$ nm/580 nm.

For WST-1 assay, the test compound was preincubated with cells for 10 min at room temperature in a 96-well plate using 100,000 cells per well, as described above, after which the reaction mixture containing 2 m*M* WST-1 plus stimuli was added. Absorbance was measured at 440 nm at a single point 45–60 min after incubation of the plate at 37°C. The pIC_{50} values for test compounds were calculated from concentration response curves using a four-parameter logistic curve fitting model.

Oxygen consumption in human PMNs and NOX4 HEK cells

Human PMNs were isolated from fresh whole blood collected from healthy volunteers as described previously (45) using Ficoll Plaque™ Plus (GE Healthcare Life Sciences) and resuspended in HBSS buffer. A Clarke electrode oximeter was prewarmed to 37°C in saturated KCl, then stabilized in HBSS for 15 min. PMNs (5×10^6 cells) were prewarmed for 5 min at 37°C with and without test compounds. Cells were then placed into the oximeter and oxygen consumption recorded for 5 min, followed by the addition of 2 μM PMA and a further 20-min recording. The oxygen content of air-saturated buffer was 240 nmol/ml. The oxygen consumption rate (OCR) was calculated from the slope of the oxygen consumption curve between 5 and 10 min.

Oxygen consumption in NOX4 T-Rex HEK cells was evaluated using the Seahorse XF24 Extracellular Flux Analyzer. NOX4 T-Rex HEK cells (50,000 cells/well) were plated onto poly-L-lysine-coated XF24 cell culture microplates (Seahorse Bioscience), treated with 1 μg/ml tetracycline, and incubated at 37°C with 5% CO_2 for 24 h. One hour before assay, the medium was changed for Dulbecco's modified Eagle's medium without carbonate buffer (D5648; Sigma-Aldrich) supplemented with 10 m*M* HEPES (Gibco), pH 7.4 (assay medium), and cells were incubated for 1 h at 37°C in normal atmosphere. The baseline OCR was recorded thrice, then rotenone (1 μM) and antimycin A (1 μM) were added in the first injection to eliminate the mitochondrial oxygen consumption component and 1 OCR cycle was measured. Test compounds were added in the second injection and 4 OCR cycles were recorded. Each OCR cycle was as follows: 3-min mixing; 2-min waiting; 3-min measuring. Data were analyzed using Wave XFe 2.1.0 software. The basal OCR in tetracycline-induced cells (before addition of blockers of mitochondrial respiration) was considered as 100% for all groups.

CFA-induced paw inflammation

Paw inflammation was induced in male C57BL6/J and $gp91^{phox}$ knockout mice by a single injection of 30 μl CFA (Sigma-Aldrich) by s.c. injection into the plantar surface of the left hind paw. Animals were anesthetized with isoflurane at 24 h after CFA injection. Each animal was then administered 25 mg/kg L-012 in 0.9% NaCl at a dose volume of 5 ml/kg *via* i.p. injection and immediately placed in a Xenogen IVIS imaging system (PerkinElmer, Inc.). Chemiluminescence in the inflamed paw was quantified with a 7-s exposure time at 0, 3, 6, 9, 12, and 15 min postinjection. The sum of chemiluminescence measured at all time points was calculated as the total chemiluminescent signal.

Test compounds were administered before L-012 injection. Apocynin (100 mg/kg, 30-min pretreatment, suspended in 2% DMSO in corn oil, dose volume of 6.6 ml/kg) and GSK2795039 (2–100 mg/kg, 60-min pretreatment, dissolved

in 20% DMSO, 20% Tween 80, 60% polyethylene glycol 200, dose volume of 2 ml/kg) were administered by i.p. injection, naloxone (50 mg/kg, 15-min pretreatment, dissolved in saline, dose volume of 5 ml/kg) by s.c. injection, and celastrol (10 mg/kg, 60-min pretreatment, suspended in 10% DMSO in 1% methylcellulose, dose volume of 5 ml/kg) by oral gavage. Chemiluminescence values for treated animals were normalized to values measured in vehicle control animals. Tail vein blood samples were collected after the IVIS imaging session for the determination of the test compound blood concentration.

Pharmacokinetic study

The pharmacokinetic parameters of GSK2795039 were determined in male SD rats (350–450 g; Animal Resources Centre) and male C57BL6/J mice (10- to 20-week-old; Biological Resource Centre, Biopolis) *via* p.o. and i.v. dosing. SD rats were prepared with a cannula inserted *via* the femoral vein into the vena cava (for compound administration) and *via* the jugular vein (for blood sampling). To determine the pharmacokinetics following i.v. administration, cannulated rats were administered an i.v. infusion of GSK2795039 in vehicle (2% DMSO, 10% hydroxy-β-cyclodextrin, 0.9% NaCl) at a dose of 1 mg/kg and at a rate of 10 ml/kg/h through the femoral cannula for 1 h. In mice, a single bolus injection of 1 mg/kg GSK2795039 was administered in the same vehicle *via* the tail vein.

To determine the pharmacokinetics following oral administration in rat, 3 mg/kg GSK2795039 was administered in 1% methylcellulose *via* oral gavage at a dose volume of 10 ml/kg. In mice, 100 mg/kg GSK2795039 was administered in 1% methylcellulose either *via* oral gavage or i.p. injection at a dose volume of 10 ml/kg. Blood samples were collected from the tail vein at various time points from 0 to 360 min. Brain tissues were also collected to determine the brain penetration of GSK2795039. The concentration of GSK2795039 in blood and tissue samples was determined by quantitative liquid chromatography, followed by mass spectrometry.

Pharmacokinetic modeling was performed using WinNonlin (Pharsight Corporation) using a noncompartmental model. Parameters obtained included C_{max}, blood clearance (Cl_b), volume of distribution (V_{ss}), and half-life ($t_{1/2}$). The oral bioavailability ($\%F_{po}$) was estimated by $(AUC_{po}/dose_{po})/(AUC_{iv}/dose_{iv}) \times 100\%$.

Mouse acute pancreatitis model

Acute pancreatitis was induced in male C57BL6/J mice using the pancreatic secretagogue, cerulein. Mice were administered 6 hourly s.c. injections of cerulein (50 μg/kg) or saline control, animals were sacrificed 1 h after the last cerulein injection, and blood samples collected. Serum was prepared *via* centrifugation of blood samples at 10,000 rpm for 5 min. GSK2795039 (100 mg/kg) or vehicle (20% DMSO, 20% Tween 80, 60% polyethylene glycol 200 vehicle) was administered twice during the protocol *via* i.p. dosing at a dose volume of 2 ml/kg. The first dose was 1 h before the first cerulein injection, and the second dose was 4 h after the first dose of compound (*i.e.*, dosing concomitantly with the fourth cerulein injection). Amylase enzyme levels were quantified in serum samples using an amylase activity assay kit (Sigma-Aldrich).

Statistics

All graphs were prepared using GraphPad Prism™ 5 or 6 and all data are expressed as mean ± standard deviation. pIC_{50} values for test compounds, except PKCB II, were calculated from concentration response curves using the XLfit (IDBS) add-in to Excel or GraphPad Prism 5. pIC_{50} values for test compounds in PKCB II were analyzed using ActivityBase XE (IDBS). Statistical analysis was performed using Statistica™ 8 (StatSoft). Data obtained from the PMN oxygen consumption assay were analyzed using a one-way ANOVA, followed by the *post hoc* Dunnett test to compare each group with control. Data obtained from CFA-induced paw inflammation assay were analyzed using a repeated measure ANOVA, followed by the *post hoc* Fisher least significant difference test. Data obtained from the acute pancreatitis assay were analyzed using a two-tailed *t*-test.

Acknowledgments

The authors would like to thank Gregory Gatto and Krista Goodman from the Metabolic Pathways and Cardiovascular Therapeutic Area (GlaxoSmithKline, USA) for their contributions to the NOX2 enzymology and lead identification, respectively; Charlotte Ashby, Philip Hardwicke, Kelvin Nurse, Rob Tanner, Oxana Polyakova, Ben Schwarz, and Monique Murray-Thompson in the Platform Technology & Sciences Department (GlaxoSmithKline, United Kingdom and USA) for their support to prepare recombinant proteins; and Andy Lockhart in the Neurodegeneration Discovery Performance Unit (GlaxoSmithKline, United Kingdom) for his support on human PBMC work. Tamara Seredenina and Vincent Jaquet are funded by the European Community Framework Programme FP7/2007-2013 under grant 278611 (Neurinox).

Author Disclosure Statement

Kazufumi Hirano, Woei Shin Chen, Angela A. Dunne, Adeline Chueng L.W., Sumitra Ramachandran, Angela Bridges, Laiq Chaudry, Gary Pettman, Craig Allan, Sarah Duncan, Kiew Ching Lee, Jean Lim, May Thu Ma, Agnes B. Ong, Nicole Y. Ye, Shabina Nasir, Sri Mulyanidewi, Chiu Cheong Aw, Pamela P. Oon, Shihua Liao, Dizheng Li, Douglas G. Johns, Neil D. Miller, Ceri H. Davies, Edward R. Browne, Yasuji Matsuoka, Deborah W. Chen, and Anthony Richard Rutter are employees of GlaxoSmithKline.

References

1. Al-Shabrawey M, Rojas M, Sanders T, Behzadian A, El-Remessy A, Bartoli M, Parpia AK, Liou G, and Caldwell RB. Role of NADPH oxidase in retinal vascular inflammation. *Invest Ophthalmol Vis Sci* 49: 3239–3244, 2008.
2. Altenhöfer S, Kleikers PW, Radermacher KA, Scheurer P, Rob Hermans JJ, Schiffers P, Ho H, Wingler K, and Schmidt HH. The NOX toolbox: validating the role of NADPH oxidases in physiology and disease. *Cell Mol Life Sci* 69: 2327–2343, 2012.
3. Altenhöfer S, Radermacher KA, Kleikers PW, Wingler K, and Schmidt HH. Evolution of NADPH oxidase inhibitors: selectivity and mechanisms for target engagement. *Antioxid Redox Signal* 23: 406–427,2015.
4. Alvarez MC, Caldiz C, Fantinelli JC, Garciarena CD, Console GM, Chiappe de Cingolani GE, and Mosca SM. Is

cardiac hypertrophy in spontaneously hypertensive rats the cause or the consequence of oxidative stress? *Hypertens Res* 31: 1465–1476, 2008.
5. Barry-Lane PA, Patterson C, van der Merwe M, Hu Z, Holland SM, Yeh ET, and Runge MS. $p47^{phox}$ is required for atherosclerotic lesion progression in $ApoE^{-/-}$ mice. *J Clin Invest* 108: 1513–1522, 2001.
6. Bechor E, Dahan I, Fradin T, Berdichevsky Y, Zahavi A, Federman Gross A, Rafalowski M, and Pick E. The dehydrogenase region of the NADPH oxidase component Nox2 acts as a protein disulfide isomerase (PDI) resembling PDIA3 with a role in the binding of the activator protein p67 (phox.). *Front Chem* 3: 3, 2015.
7. Bedard K and Krause KH. The NOX family of ROS-generating NADPH oxidases: physiology and pathophysiology. *Physiol Rev* 87: 245–313, 2007.
8. Bhandarkar SS, Jaconi M, Fried LE, Bonner MY, Lefkove B, Govindarajan B, Perry BN, Parhar R, Mackelfresh J, Sohn A, Stouffs M, Knaus U, Yancopoulos G, Reiss Y, Benest AV, Augustin HG, and Arbiser JL. Fulvene-5 potently inhibits NADPH oxidase 4 and blocks the growth of endothelial tumors in mice. *J Clin Invest* 119: 2359–2365, 2009.
9. Bolscher BG, van Zwieten R, Kramer IM, Weening RS, Verhoeven AJ, and Roos D. A phosphoprotein of Mr 47,000, defective in autosomal chronic granulomatous disease, copurifies with one of two soluble components required for NADPH:O_2 oxidoreductase activity in human neutrophils. *J Clin Invest* 83: 757–763, 1989.
10. Carnesecchi S, Deffert C, Donati Y, Basset O, Hinz B, Preynat-Seauve O, Guichard C, Arbiser JL, Banfi B, Pache JC, Barazzone-Argiroffo C, and Krause KH. A key role for NOX4 in epithelial cell death during development of lung fibrosis. *Antioxid Redox Signal* 15: 607–619, 2011.
11. Chacko BK, Kramer PA, Ravi S, Johnson MS, Hardy RW, Ballinger SW, and Darley-Usmar VM. Methods for defining distinct bioenergetic profiles in platelets, lymphocytes, monocytes, and neutrophils, and the oxidative burst from human blood. *Lab Invest* 93: 690–700, 2013.
12. Cifuentes-Pagano E, Csanyi G, and Pagano PJ. NADPH oxidase inhibitors: a decade of discovery from Nox2ds to HTS. *Cell Mol Life Sci* 69: 2315–2325, 2012.
13. Cleren C, Calingasan NY, Chen J, and Beal MF. Celastrol protects against MPTP- and 3-nitropropionic acid-induced neurotoxicity. *J Neurochem* 94: 995–1004, 2005.
14. Cross AR and Jones OT. The effect of the inhibitor diphenylene iodonium on the superoxide-generating system of neutrophils. Specific labelling of a component polypeptide of the oxidase. *Biochem J* 237: 111–116, 1986.
15. Diebold BA, Smith SM, Li Y, and Lambeth JD. NOX2 as a target for drug development: indications, possible complications, and progress. *Antioxid Redox Signal* 23: 375–405, 2015.
16. Dikalov SI and Harrison DG. Methods for detection of mitochondrial and cellular reactive oxygen species. *Antioxid Redox Signal* 20: 372–382, 2014.
17. Dulu TD, Kanui TI, Towett PK, Maloiy GM, and Abelson KS. The effects of oxotremorine, epibatidine, atropine, mecamylamine and naloxone in the tail-flick, hot-plate, and formalin tests in the naked mole-rat (*Heterocephalus glaber*). In Vivo 28: 39–48, 2014.
18. Fornwald JA, Lu Q, Wang D, and Ames RS. Gene expression in mammalian cells using BacMam, a modified baculovirus system. *Methods Mol Biol* 388: 95–114, 2007.
19. Gade SK, Bhattacharya S, and Manoj KM. Redox active molecules cytochrome c and vitamin C enhance heme-enzyme peroxidations by serving as non-specific agents for redox relay. *Biochem Biophys Res Commun* 419: 211–214, 2012.
20. Gatley SJ and Martin JL. Some aspects of the pharmacology of diphenyleneiodonium, a bivalent iodine compound. *Xenobiotica* 9: 539–546, 1979.
21. Gatto GJ, Jr., Ao Z, Kearse MG, Zhou M, Morales CR, Daniels E, Bradley BT, Goserud MT, Goodman KB, Douglas SA, Harpel MR, and Johns DG. NADPH oxidase-dependent and -independent mechanisms of reported inhibitors of reactive oxygen generation. *J Enzyme Inhib Med Chem* 28: 95–104, 2013.
22. Genovese T, Mazzon E, Paterniti I, Esposito E, Bramanti P, and Cuzzocrea S. Modulation of NADPH oxidase activation in cerebral ischemia/reperfusion injury in rats. *Brain Res* 1372: 92–102, 2011.
23. Gianni D, Taulet N, Zhang H, DerMardirossian C, Kister J, Martinez L, Roush WR, Brown SJ, Bokoch GM, and Rosen H. A novel and specific NADPH oxidase-1 (Nox1) small-molecule inhibitor blocks the formation of functional invadopodia in human colon cancer cells. *ACS Chem Biol* 5: 981–993, 2010.
24. Gill PS and Wilcox CS. NADPH oxidases in the kidney. *Antioxid Redox Signal* 8: 1597–1607, 2006.
25. Gorin Y, Block K, Hernandez J, Bhandari B, Wagner B, Barnes JL, and Abboud HE. Nox4 NAD(P)H oxidase mediates hypertrophy and fibronectin expression in the diabetic kidney. *J Biol Chem* 280: 39616–39626, 2005.
26. Gukovskaya AS, Vaquero E, Zaninovic V, Gorelick FS, Lusis AJ, Brennan M-L, Holland S and Pandol SJ. Neutrophils and NADPH oxidase mediate intrapancreatic trypsin activation in murine experimental acute pancreatitis. *Gastroenterology* 122: 974–984, 2002.
27. Heumüller S, Wind S, Barbosa-Sicard E, Schmidt HH, Busse R, Schröder K, and Brandes RP. Apocynin is not an inhibitor of vascular NADPH oxidases but an antioxidant. *Hypertension* 51: 211–217, 2008.
28. Hua H, Munk S, Goldberg H, Fantus IG, and Whiteside CI. High glucose-suppressed endothelin-1 Ca^{2+} signaling via NADPH oxidase and diacylglycerol-sensitive protein kinase C isozymes in mesangial cells. *J Biol Chem* 278: 33951–33962, 2003.
29. Imai Y, Kuba K, Neely GG, Yaghubian-Malhami R, Perkmann T, van Loo G, Ermolaeva M, Veldhuizen R, Leung YH, Wang H, Liu H, Sun Y, Pasparakis M, Kopf M, Mech C, Bavari S, Peiris JS, Slutsky AS, Akira S, Hultqvist M, Holmdahl R, Nicholls J, Jiang C, Binder CJ, and Penninger JM. Identification of oxidative stress and Toll-like receptor 4 signaling as a key pathway of acute lung injury. *Cell* 133: 235–249, 2008.
30. Jaquet V, Marcoux J, Forest E, Leidal KG, McCormick S, Westermaier Y, Perozzo R, Plastre O, Fioraso-Cartier L, Diebold B, Scapozza L, Nauseef WM, Fieschi F, Krause KH, and Bedard K. NADPH oxidase (NOX) isoforms are inhibited by celastrol with a dual mode of action. *Br J Pharmacol* 164: 507–520, 2011.
31. Jaquet V, Scapozza L, Clark RA, Krause KH, and Lambeth JD. Small-molecule NOX inhibitors: ROS-generating NADPH oxidases as therapeutic targets. *Antioxid Redox Signal* 11: 2535–2552, 2009.
32. Judkins CP, Diep H, Broughton BR, Mast AE, Hooker EU, Miller AA, Selemidis S, Dusting GJ, Sobey CG, and

Drummond GR. Direct evidence of a role for Nox2 in superoxide production, reduced nitric oxide bioavailability, and early atherosclerotic plaque formation in ApoE$^{-/-}$ mice. *Am J Physiol Heart Circ Physiol* 298: H24–H32, 2010.
33. Kawahara T, Quinn MT, and Lambeth JD. Molecular evolution of the reactive oxygen-generating NADPH oxidase (Nox/Duox) family of enzymes. *BMC Evol Biol* 7: 109, 2007.
34. Kedare SB and Singh RP. Genesis and development of DPPH method of antioxidant assay. *J Food Sci Technol* 48: 412–422, 2011.
35. Kiaei M, Kipiani K, Petri S, Chen J, Calingasan NY, and Beal MF. Celastrol blocks neuronal cell death and extends life in transgenic mouse model of amyotrophic lateral sclerosis. *Neurodegener Dis* 2: 246–254, 2005.
36. Lambeth JD. Nox enzymes, ROS, and chronic disease: an example of antagonistic pleiotropy. *Free Radic Biol Med* 43: 332–347, 2007.
37. Lambeth JD, Kawahara T, and Diebold B. Regulation of Nox and Duox enzymatic activity and expression. *Free Radic Biol Med* 43: 319–331, 2007.
38. Lambeth JD and Neish AS. Nox enzymes and new thinking on reactive oxygen: a double-edged sword revisited. *Annu Rev Pathol* 9: 119–145, 2014.
39. Le Cabec V and Maridonneau-Parini I. Complete and reversible inhibition of NADPH oxidase in human neutrophils by phenylarsine oxide at a step distal to membrane translocation of the enzyme subunits. *J Biol Chem* 270: 2067–2073, 1995.
40. Liu B, Jiang JW, Wilson BC, Du L, Yang SN, Wang JY, Wu GC, Cao XD, and Hong JS. Systemic infusion of naloxone reduces degeneration of rat substantia nigral dopaminergic neurons induced by intranigral injection of lipopolysaccharide. *J Pharmacol Exp Ther* 295: 125–132, 2000.
41. Liu J, Zhou J, An W, Lin Y, Yang Y, and Zang W. Apocynin attenuates pressure overload-induced cardiac hypertrophy in rats by reducing levels of reactive oxygen species. *Can J Physiol Pharmacol* 88: 745–752, 2010.
42. Maghzal GJ, Krause KH, Stocker R, and Jaquet V. Detection of reactive oxygen species derived from the family of NOX NADPH oxidases. *Free Radic Biol Med* 53: 1903–1918, 2012.
43. Martinez RM, Zarpelon AC, Cardoso RD, Vicentini FT, Georgetti SR, Baracat MM, Andrei CC, Moreira IC, Verri WA, Jr., and Casagrande R. Tephrosia sinapou ethyl acetate extract inhibits inflammatory pain in mice: opioid receptor dependent inhibition of TNFα and IL-1β production. *Pharm Biol* 51: 1262–1271, 2013.
44. Munson JM, Fried L, Rowson SA, Bonner MY, Karumbaiah L, Diaz B, Courtneidge SA, Knaus UG, Brat DJ, Arbiser JL, and Bellamkonda RV. Anti-invasive adjuvant therapy with imipramine blue enhances chemotherapeutic efficacy against glioma. *Sci Transl Med* 4: 127ra36, 2012.
45. Nauseef WM. Isolation of human neutrophils from venous blood. *Methods Mol Biol* 412: 15–20, 2007.
46. Nayernia Z, Jaquet V, and Krause KH. New insights on NOX enzymes in the central nervous system. *Antioxid Redox Signal* 20: 2815–2837, 2014.
47. Nwokocha CR, Baker A, Douglas D, McCalla G, Nwokocha M, and Brown PD. Apocynin ameliorates cadmium-induced hypertension through elevation of endothelium nitric oxide synthase. *Cardiovasc Toxicol* 13: 357–363, 2013.
48. O'Donnell BV, Tew DG, Jones OT, England PJ. Studies on the inhibitory mechanism of iodonium compounds with special reference to neutrophil NADPH oxidase. *Biochem J* 290: 41–49, 1993.
49. O'Donnell VB, Smith GC, and Jones OT. Involvement of phenyl radicals in iodonium inhibition of flavoenzymes. *Mol Pharmacol* 46: 778–785, 1994.
50. Rada B and Leto TL. Oxidative innate immune defenses by Nox/Duox family NADPH oxidases. *Contrib Microbiol* 15: 164–187, 2008.
51. Repine JE, White JG, Clawson CC, and Holmes BM. Effects of phorbol myristate acetate on the metabolism and ultrastructure of neutrophils in chronic granulomatous disease. *J Clin Invest* 54: 83–90, 1974.
52. Selemidis S, Sobey CG, Wingler K, Schmidt HH, and Drummond GR. NADPH oxidases in the vasculature: molecular features, roles in disease and pharmacological inhibition. *Pharmacol Ther* 120: 254–291, 2008.
53. Seredenina T, Chiriano G, Filippova A, Nayernia Z, Mahiout Z, Fioraso-Cartier L, Plastre O, Scapozza L, Krause KH, and Jaquet V. A subset of N-substituted phenothiazines inhibits NADPH oxidases. *Free Radic Biol Med* 2015; DOI: 10.1016/j.freeradbiomed.2015.05.023.
54. Serrander L, Cartier L, Bedard K, Banfi B, Lardy B, Plastre O, Sienkiewicz A, Forro L, Schlegel W, and Krause KH. NOX4 activity is determined by mRNA levels and reveals a unique pattern of ROS generation. *Biochem J* 406: 105–114, 2007.
55. Shaker ME, Ashamallah SA, and Houssen ME. Celastrol ameliorates murine colitis via modulating oxidative stress, inflammatory cytokines and intestinal homeostasis. *Chem Biol Interact* 210: 26–33, 2014.
56. Sheehan AL, Carrell S, Johnson B, Stanic B, Banfi B, and Miller FJ, Jr. Role for Nox1 NADPH oxidase in atherosclerosis. *Atherosclerosis* 216: 321–326, 2011.
57. Simons JM, Hart BA, Ip Vai Ching TR, Van Dijk H, and Labadie RP. Metabolic activation of natural phenols into selective oxidative burst agonists by activated human neutrophils. *Free Radic Biol Med* 8: 251–258, 1990.
58. Smith SM, Min J, Ganesh T, Diebold B, Kawahara T, Zhu Y, McCoy J, Sun A, Snyder JP, Fu H, Du Y, Lewis I, and Lambeth JD. Ebselen and congeners inhibit NADPH oxidase 2-dependent superoxide generation by interrupting the binding of regulatory subunits. *Chem Biol* 19: 752–763, 2012.
59. Stefanska J and Pawliczak R. Apocynin: molecular aptitudes. *Mediators Inflamm* 2008: 106507, 2008; DOI: 10.1155/2008/106507.
60. Stein CA. Suramin: a novel antineoplastic agent with multiple potential mechanisms of action. *Cancer Res* 53: 2239–2248, 1993.
61. Tan AS and Berridge MV. Superoxide produced by activated neutrophils efficiently reduces the tetrazolium salt, WST-1 to produce a soluble formazan: a simple colorimetric assay for measuring respiratory burst activation and for screening anti-inflammatory agents. *J Immunol Methods* 238: 59–68, 2000.
62. Tang XN, Cairns B, Cairns N, and Yenari MA. Apocynin improves outcome in experimental stroke with a narrow dose range. *Neuroscience* 154: 556–562, 2008.
63. Thelen M, Dewald B, and Baggiolini M. Neutrophil signal transduction and activation of the respiratory burst. *Physiol Rev* 73: 797–821, 1993.
64. Tucker KA, Lilly MB, Heck L, Jr., and Rado TA. Characterization of a new human diploid myeloid leukemia cell

line (PLB-985) with granulocytic and monocytic differentiating capacity. *Blood* 70: 372–378, 1987.
65. Wang Q, Zhou H, Gao H, Chen SH, Chu CH, Wilson B, and Hong JS. Naloxone inhibits immune cell function by suppressing superoxide production through a direct interaction with gp91phox subunit of NADPH oxidase. *J Neuroinflammation* 9: 32, 2012.
66. Wu DC, Ré DB, Nagai M, Ischiropoulos H, and Przedborski S. The inflammatory NADPH oxidase enzyme modulates motor neuron degeneration in amyotrophic lateral sclerosis mice. *Proc Natl Acad Sci U S A* 103: 12132–12137, 2006.
67. Yoshida LS, Abe S, and Tsunawaki S. Fungal gliotoxin targets the onset of superoxide-generating NADPH oxidase of human neutrophils. *Biochem Biophys Res Commun* 268: 716–723, 2000.
68. Zhen L, King AA, Xiao Y, Chanock SJ, Orkin SH, and Dinauer MC. Gene targeting of X chromosome-linked chronic granulomatous disease locus in a human myeloid leukemia cell line and rescue by expression of recombinant gp91phox. *Proc Natl Acad Sci U S A* 90: 9832–9836, 1993.
69. Zielonka J, Lambeth JD, and Kalyanaraman B. On the use of L-012, a luminol-based chemiluminescent probe, for detecting superoxide and identifying inhibitors of NADPH oxidase: a re-evaluation. *Free Radic Biol Med* 65: 1310–1314, 2013.

Address correspondence to:
Dr. A. Richard Rutter
Neural Pathways Discovery Performance Unit
Neurosciences Therapeutic Area
GlaxoSmithKline
Biopolis
11 Biopolis Way
The Helios #06-03
Singapore 138667
Singapore

E-mail: richard.a.rutter@gsk.com

Date of first submission to ARS Central, November 19, 2014; date of final revised submission, June 19, 2015; date of acceptance, June 29, 2015.

Abbreviations Used

AUC = area under the curve
BHK = baby hamster kidney
Cl_b = blood clearance
C_{max} = peak blood concentration
CFA = complete Freund's adjuvant
CHAPS = 3-[(3-cholamidopropyl)dimethylammonio]-1-propanesulfonate
DMSO = dimethyl sulfoxide
DPI = diphenyleneiodonium
DPPH = 2,2-diphenyl-1-picrylhydrazyl
DUOX = dual oxidase
EGTA = ethylene glycol-bis(2-aminoethylether)-*N*,*N*,*N*′,*N*′-tetraacetic acid
eNOS = endothelial nitric oxide synthase
FAD = flavin adenine dinucleotide
FBS = fetal bovine serum
F_{po} = oral bioavailability
GTPγS = guanosine 5′-O-(3-thiotriphosphate)
HBSS = Hank's balanced salt solution
HEK = human embryonic kidney
HRP = horseradish peroxidase
i.p. = intraperitoneal
i.v. = intravenous
K_m = Michaelis constant
NOX = NADPH oxidase
OCR = oxygen consumption rate
PBMC = peripheral blood mononucleated cell
PBS = phosphate-buffered saline
PKC = protein kinase C
PKCB II = protein kinase C beta2
PMA = phorbol 12-myristate 13-acetate
PMNs = polymorphonuclear leukocytes
p.o. = oral administration
ROS = reactive oxygen species
s.c. = subcutaneous
SD = Sprague-Dawley
SDS = sodium dodecyl sulfate
$t_{1/2}$ = half-life
V_{max} = maximum enzyme velocity
V_{ss} = steady-state volume of distribution
WST-1 = water-soluble tetrazolium salt1